


5-1-2022

Towards Highly Sensitive Capacitance Measurements of a Quantum Anomalous Hall Phase in Van Der Waal Heterostructures

Kayla Cerminara

Follow this and additional works at: <https://digitalscholarship.unlv.edu/thesesdissertations>

 Part of the [Condensed Matter Physics Commons](#), and the [Nanoscience and Nanotechnology Commons](#)

Repository Citation

Cerminara, Kayla, "Towards Highly Sensitive Capacitance Measurements of a Quantum Anomalous Hall Phase in Van Der Waal Heterostructures" (2022). *UNLV Theses, Dissertations, Professional Papers, and Capstones*. 4381.
<http://dx.doi.org/10.34917/31813261>

This Thesis is protected by copyright and/or related rights. It has been brought to you by Digital Scholarship@UNLV with permission from the rights-holder(s). You are free to use this Thesis in any way that is permitted by the copyright and related rights legislation that applies to your use. For other uses you need to obtain permission from the rights-holder(s) directly, unless additional rights are indicated by a Creative Commons license in the record and/or on the work itself.

This Thesis has been accepted for inclusion in UNLV Theses, Dissertations, Professional Papers, and Capstones by an authorized administrator of Digital Scholarship@UNLV. For more information, please contact digitalscholarship@unlv.edu.

TOWARDS HIGHLY SENSITIVE CAPACITANCE MEASUREMENTS OF A
QUANTUM ANOMALOUS HALL PHASE IN VAN DER WAAL
HETEROSTRUCTURES

By

Kayla Cerminara

Bachelor of Science – Physics
University of Nevada, Las Vegas
2020

A thesis submitted in partial fulfillment
of the requirements for the

Master of Science – Physics

Department of Physics and Astronomy
College of Sciences
The Graduate College

University of Nevada, Las Vegas
May 2022



Thesis Approval

The Graduate College
The University of Nevada, Las Vegas

April 7, 2022

This thesis prepared by

Kayla Cerminara

entitled

Towards Highly Sensitive Capacitance Measurements of a Quantum Anomalous Hall
Phase in Van Der Waal Heterostructures

is approved in partial fulfillment of the requirements for the degree of

Master of Science – Physics
Department of Physics and Astronomy

Joshua Island, Ph.D.
Examination Committee Chair

Andrew Cornelius, Ph.D.
Examination Committee Member

Tao Pang, Ph.D.
Examination Committee Member

Marykay Orgill, Ph.D.
Graduate College Faculty Representative

Kathryn Hausbeck Korgan, Ph.D.
*Vice Provost for Graduate Education &
Dean of the Graduate College*

Abstract

One of the pioneering achievements in condensed matter physics of the 20th century is the observation of the quantum Hall effect (QHE) in which the Hall resistance in a two-dimensional (2D) sample takes on quantized values in the presence of a strong perpendicular magnetic field. The precise quantization of the hall resistance to one part in a billion has provided a practical, worldwide resistance standard. A long-standing goal has been to realize a similar state of matter but without the need of a strong quantizing magnetic field. The quantum anomalous Hall effect (QAHE) is such a state that is predicted to exist in 2D materials with intrinsic magnetism and strong spin orbit coupling. Very few materials have these inherent properties, but new materials can be synthetically engineered by stacking and combining 2D layers into heterostructures with desired characteristics. In this thesis, we work toward combining graphene and few-layer graphene with materials that exhibit strong spin orbit coupling (molybdenum disulfide) with the goal of realizing a robust QAHE. To ascertain the presence of a zero-field gap in the electronic spectrum of the material, a benchmark of the QAHE, we implement a highly sensitive capacitance measurement technique. We present theoretical background on the quantum Hall effects and capacitance measurements to begin. We then present fabrication and measurements of four devices, two incorporating single layer graphene and two with bilayer graphene. Our work opens the door to prospective devices with utility in spintronics and topological quantum computing.

Table of Contents

Abstract	iii
Table of Contents	iv
List of Figures	vi
Chapter 1 Introduction	1
Chapter 2 Theoretical Background	4
2.1 The Hall Effects	4
2.1.1 Hall Effect	4
2.1.2 Quantum Hall Effect	7
2.1.3 Anomalous Hall Effect	7
2.1.4 Quantum Anomalous Hall Effect	8
2.2 Capacitance	8
2.3 Material Theory	12
2.3.1 Graphene	12
2.3.2 Molybdenum Disulfide	14
2.3.3 Hexagonal Boron Nitride	15
Chapter 3 Fabrication Processes for Capacitance Devices	16
3.1 Stack Design	16
3.1.1 Exfoliation	17
3.1.2 Stacking	19
3.2 Photolithography	21

3.3 Etching	25
Chapter 4 Instrumentation and Measurement	29
4.1 Instrumentation	29
4.1.1 Capacitance Bridge	29
4.1.2 Cryostat to Measurement Electronics	31
4.2 Capacitance Measurements	32
Chapter 5 Results	33
5.1 Monolayer Graphene on MoS ₂	34
5.2 Bilayer Graphene on MoS ₂	38
Chapter 6 Discussion and Future Work	43
Appendix	46
Bibliography	62
Curriculum Vitae	66

List of Figures

1.1	Theoretical calculations of the band structure of the predicted QAHE in bilayer graphene. Figure adapted from [1]. (a) A schematic of a van der Waals heterostructure of bilayer graphene sandwiched between a layer of a ferromagnetic insulator and a spin orbit coupling material (top left). The rest of the images are plots of the band structure of the theoretically predicted valley-polarized quantum anomalous Hall effect where the red (blue) band indicates the up (down) spins. (b) The band structure of a finite-sized 25 nm wide nanoribbon of the heterostructure shown in (a). The red bands represent the topological edge states and the gray shaded area is where the Hall resistance is predicted to be quantized at h/e^2	2
2.1	The Hall effect occurs when a voltage is measured in the x-direction while a current is applied in the y-direction. This happens under the condition that there is an applied magnetic field in the z-direction.	5

2.2	The Hall effect and 3 of its analogues. (a) The Hall effect: the Lorenz force acting on the electrons in the presence of a magnetic field going into the page. (b) The Quantum Hall effect: The electrons undergo skipping orbits at the boundaries and the other states are localized in cyclotron orbits within the middle. (c) Anomalous Hall effect: The material acts the same as the hall effect, except without an applied magnetic field. (d) Quantum Anomalous Hall effect: The quantum Hall effect without the presence of an external magnetic field.	6
2.3	(a) Example of a device used for capacitance measurements. Labeled are the source and the drain to the device, the material being probed or the channel, an insulating material, and a gate voltage applied to the bottom. (b-c) Plots of the density of states of a two band semiconductor for different gate voltages. The red line, μ , indicates the electrostatic chemical potential. (b) The density of states with no gate voltage. (c) When a negative voltage is applied to the device. The conduction band will move to be in line with μ . (d) When Fermi level is moved inside the the conduction band, the material becomes conducting.	9
2.4	Graphene crystal structure and energy band structure. Figure adapted from Castro Neto et al. [2]. (a) The crystal structure for monolayer graphene. It is a honeycomb lattice made up of carbon atoms. (b) The crystal structure for multiple layers of graphite is monolayer graphene stacked on top of itself. (c) Graphene's band structure with hopping values of $t = 2.7eV$ and $t' = -0.2t$. The inset shows a zoomed in picture of one of the Dirac cones.	12
2.5	The theoetical band structure of MoS_2 , calculated from first priciples. This figure is adapted from [3]. (a) The d orbital contribution. (b) The p orbital contribution. (c) The s orbital contribution.	14

2.6	The crystal structure[4] and the band structure[5] of hBN. (a) Multi-layer BN is similar to graphite in that the bulk structure is composed of monolayers stacked on top of one another. (b) Monolayer BN has the same hexagonal or honeycomb structure as graphene. (c) The LDA (local density approximation) band structure of bulk hBN. (d) The GW (Coulomb-Green's function approximation) band structure of bulk hBN.	15
3.1	Overview of the stack design and etching. (a) A model of a representative heterostructure. There are two graphite gates on the top and the bottom of the stack. There is then an insulating layer of material next to the gates, with the graphene and MoS ₂ in the middle. (b) An optical image of a stack before the etching process. (c) An optical image of the same stack after the excess material has been etched away.	17
3.2	Optical microscopy images of various flakes of materials that have been exfoliated using the Scotch tape method. These include: (a) Flake of BN that is used as the first pick up layer due to the large surface area. BN is also used as an insulating layer in between stack. (b) Flake of graphite that was used as a top gate. The graphite that is used for gates is typically > 5 layers. (c) Flake of bilayer graphene (d) Flake of MoS ₂ . MoS ₂ is used with graphene due to its larger spin orbit coupling energy.	19

3.3 Overview of the stacking process that is used to fabricate the devices that we use for capacitance measurements. The first row of figures shows how the first piece of BN is picked up using adhesion forces from household nail polish. The second row of panels shows how later flakes are stacked using the van der Waals forces between the materials. The last row of images is how the stack is transferred to a substrate of choice. (a) At the top is the glass slide with the hemisphere, in blue, that is created by layering a piece of clear tape over a cylinder of PDMS. A drop of nail polish is then put on the top of the hemisphere. At the bottom shows a flake of BN that has been found on top of a Si/SiO₂ chip. (b) The glass slide is slowly lowered over top of the flake using the z-axis on the micromanipulator. The nail polish drop then pins a corner of a flake of material and is continuously brought down until the flake has been covered. (c) The slide is pulled up quickly, taking the flake of material with it. (d) The slide with the BN is positioned over the next flake of material. (e) The slide is slowly lowered pinning a corner of a flake of material with the BN. Heat is applied from the stage in increments of 2°C until the flake is covered by the BN and nail polish. This happens around 48°C. (f) The heat is then lowered back to 40°C and the z-axis is used to slowly bring up the picked up flake. The materials should now be stacked on top of each other. (g) To transfer the whole stack, the slide is positioned in reference to the electrode position on the chip that the stack will be transferred to. (e) The slide is lowered and a corner of the stack is pinned to the substrate. The heat is raised in increments of 20°C. The z-axis is used to keep the nail polish from laminating the while chip and keeping the nail polish to the area around the stack. The heat is stopped once it reaches 110°C. (f) The heat is held at 110°C while the z-axis is used to slowly pull up the glass slide. 22

3.4	Optical images of a device after the photolithography processing and after gold electrodes have been deposited. (a-b) A mask is applied to the device using photolithography techniques. This mask is a single layer of photoresist. The brown regions are the exposed substrate surface after development and the green regions show where the resist still resides. (c-d) Gold is deposited to the chip using an electron beam deposition. The resist mask is removed using acetone and the gold electrodes are left where the photoresist was exposed.	26
3.5	Optical images of a stack undergoing an etching process. (a) An optical image of the stack before the copper mask has been deposited. (b) The stack after the copper mask has been deposited, before etching has started. Images (c-i) are after different etching formulas for the different materials: (c) BN, (d) Gr, (e) BN, (f) Gr, (g) MoS ₂ , (h) BN, and (i) Gr. The last image (j) shows the stack after the copper mask has been removed.	28
4.1	Schematic of the electrical setup used to make the capacitance measurements. The red outlined portion represents the electronics and device that are located inside the cryostat. See the main text for further descriptions.	30

- 5.1 This figure shows data that was obtained from device JMA002. (a) An optical image of the device with patterned gold electrodes. (b) A digitally drawn schematic of the layers of JMA002. There is monolayer graphene in contact with MoS₂. These two materials are sandwiched on each side by BN and graphite gates. (c) 2D plot of the penetration capacitance (C_p), scaled by the reference capacitor (C_{ref}), plotted as a function of charge concentration (n_0/c) and polarization (p_0/c) taken at 2 K. (d) A line cut taken of plot in (c) at $p_0 = 7V$. The peak is due to the reduction in the DOS of the graphene flake. (e) 2D plot of C_p/C_{ref} as a function of n_0/c and p_0/c taken at 2 K and 9 T magnetic field. The plot shows the quantum hall gaps as vertical lines starting in the middle at 0 V and working outwards. (f) A line cut of plot of the data plotted in (e) taken at $p_0 = 5$ V. The filling factors can be seen as local maxima, starting at 0 V and working outwards. 35
- 5.2 This figure shows the data that was obtained for device KC011. (a) An optical image of the device. (b) A digitally drawn schematic of the layers of KC011. There is monolayer graphene that is in contact with MoS₂. These two materials are sandwiched on each side by BN and graphite gates. (c) 2D plot of the penetration capacitance (C_p), scaled by the reference capacitor (C_{ref}), plotted as a function of charge concentration (n_0/c) and polarization (p_0/c) taken at 2 K. (d) A line cut of the data plotted in (c) at a polarization of 4 V. (e) 2D plot of the penetration capacitance (C_p), scaled by the reference capacitor (C_{ref}), plotted as a function of charge concentration (n_0/c) and polarization (p_0/c) taken at 2 K and 9 T. The quantum hall gaps show up in the plot as vertical lines, starting with 0 at $n_0/c = 0$ V and working outwards. (f) A line cut taken from plot (e) at $p_0/c = 5$ V. The quantum hall gaps can be seen as local maxima start in the middle at $n_0/c = 0$ V and working outwards. 37

5.3	The room temperature (300 K) data taken for KC004 at no external magnetic field (0 T). (a) An optical image of the device. (b) A schematic of the layers of KC004. There is bilayer graphene flake in contact with MoS ₂ that has been sandwiched on each side by a piece of BN and graphite. (c) A 2D plot with the penetration capacitance (C_p) scaled by the reference capacitance (C_{ref}) of the capacitance bridge as a function of the charge concentration (n_0/c) and the polarization (p_0/c). The difference between the red and the blue shows the conduction band edge of the MoS ₂ where the right side of the graph is the conduction band. (d) A line cut taken of the data plotted in (c) taken at $p_0/c = 5$ V.	39
5.4	The data taken for KC004 at 2K with no external magnetic field. (a) The data for the scaled capacitance measurements as a function of charge concentration and polarization. The band edge of MoS ₂ can be seen, but it is vertical. (b) A line cut taken of plot (a) taken at $n_0/c = 5$ V shows that the relationship is linear. (c) The background of plot (a) was subtracted by taking a line cut at $n_0/c = -5$ V and then subtracted from the rest of the lines of the plot. This gives us the expected vertical line of the MoS ₂ and the band edge. The band gap of the bilayer graphene can also be seen as the slight yellow line. (d) A line cut was taken at $p_0/c = 5$ V of plot (c). At $n_0/c = 0$ V, there is a sharp peak from the band gap of the graphene. The red line then declines around $n_0/c = 2$ V indicating the MoS ₂ band edge.	41

5.5	The data taken for the device JMA003. (a) An optical image of the device with the patterned electrodes. (b) A layer schematic of the device. This device has bilayer graphene in contact with MoS ₂ that is sandwiched between BN and graphite on both sides. (c) A 2D plot taken at 2 K with no applied magnetic field (0 T). It shows the penetration capacitance scaled by the reference capacitance of the capacitance bridge (C_p/C_{ref}) as a function of the charge concentration (n_0/c) and the polarization (p_0/c). The band edge of the MoS ₂ can be seen on the right of the graph, represented by the change in colors from red to blue. (d) A line cut of plot (c) taken at $p_0/c = -3$ V. This shows the band gap of the graphene around $n_0/c = -0.5$ V as the sharp peak. The band edge of the MoS ₂ is seen around $n_0/c = 1.5$ V indicated by the decline. (e) C_p/C_{ref} as a function of n_0/c and p_0/c taken for the device at a temperature of 2 K and with an applied magnetic field of 9 T. This plot shows the quantum Hall gaps of the bilayer graphene. (f) A line cut taken of plot (e) at $p_0/c = -5$ V. The local maxima are the quantum Hall gaps of the bilayer graphene.	42
6.1	The degradation in ambient conditions and passivation of Chromium triiodide(CrI ₃). Panel (a-c) are optical images of CrI ₃ in ambient conditions taken at (a) 10 minutes, (b) 15 minutes, and (c) 50 minutes. Panel (d-f) are optical images of CrI ₃ after being layered by BN taken at (d) 10 minutes, (e) 15 minutes, and (f) 50 minutes in ambient conditions.	44

Chapter 1

Introduction

The quantum anomalous Hall effect (QAHE) is a robust, topologically protected phase of matter that has great potential in the fields of electronics, spintronics, and quantum computing [6] [7] [8] [9]. In contrast with the well known quantum Hall effect[10], the QAHE presents quantized resistances without the need of a high magnetic field, an impractical requirement for the above mentioned applications. In order for a material to exhibit the QAHE, it needs to have intrinsic magnetism and a significant spin orbit coupling (SOC) energy[11, 12, 13, 14]. Very few two-dimensional materials possess these attributes and the QAHE was first observed in a very complex system ($\text{Cr}_{0.15}(\text{Bi}_{0.1}\text{Sb}_{0.9})_{1.85}\text{Te}_3$) grown by molecular beam epitaxy[15]. It would be advantageous to discover a more readily available, abundant material with these attractive properties.

Graphene, a single layer of graphite, has been a material of great interest due to its structural strength and its ability to allow electrons to easily flow through it (high mobility) [16]. Unfortunately, in graphene the SOC strength is very small and results in a minuscule electronic gap of $42 \mu\text{eV}$ [17] and it is also not intrinsically magnetic. This means graphene is not predicted to possess a QAHE on its own. Fortunately, it is possible to combine graphene with other materials by forming van der Waals heterostructures [18]. In these heterostructures, the adjoining materials can lend their properties to graphene

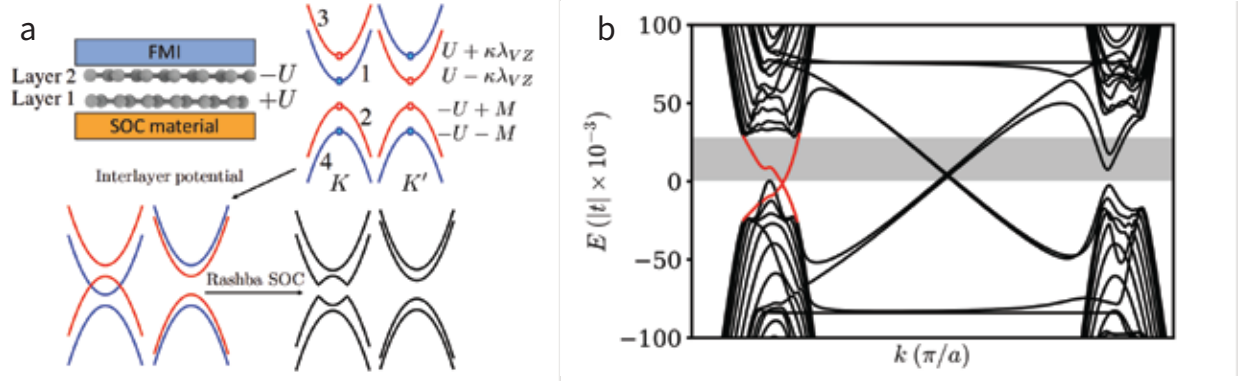


Figure 1.1: Theoretical calculations of the band structure of the predicted QAHE in bilayer graphene. Figure adapted from [1]. (a) A schematic of a van der Waals heterostructure of bilayer graphene sandwiched between a layer of a ferromagnetic insulator and a spin orbit coupling material (top left). The rest of the images are plots of the band structure of the theoretically predicted valley-polarized quantum anomalous Hall effect where the red (blue) band indicates the up (down) spins. (b) The band structure of a finite-sized 25 nm wide nanoribbon of the heterostructure shown in (a). The red bands represent the topological edge states and the gray shaded area is where the Hall resistance is predicted to be quantized at h/e^2 .

through proximity effects [19, 20]. It has been predicted that a QAHE can exist in bilayer graphene (two layers of graphene) if it is sandwiched between a ferromagnetic insulator (FMI) and a strong SOC semiconductor[1]. In figure 1.1 the predicted theoretical band structure is shown for the heterostructure. A model of the heterostructure is shown in figure 1.1(a) along with the conduction and valence bands of the band structure. Magnetism from the FMI splits the valence band degeneracy and SOC from the semiconductor splits the conduction band degeneracy (top right panel of figure 1.1(a)). By tuning the interlayer potential, U , with a perpendicular electrical field (provided by electrostatic gates), the bands with opposite spin can be made to overlap (bottom left panel of figure 1.1(a)). With the addition of Rashba SOC, these bands hybridize and result in an inverted gap (bottom right panel of figure 1.1(a)). In a finite sized system (with edges) theoretical calculations predict edge states, the red bands in figure 1.1(b), that result in a quantized Hall resistance, a QAHE.

To determine the presence of the predicted hybridized gap, we employ sensitive capacitance measurements in this work. Capacitance measurements give information about a material's electronic structure through the thermodynamic density of states, $dn/d\mu$, where n is the charge density and μ is the chemical potential[21, 22, 23]. This is helpful in the study of two dimensional materials including being able to easily and clearly detect electronic energy gaps, such as the one predicted for the QAHE in bilayer graphene. With the set up presented in this thesis, the capacitance measurements can probe individual layers of the van der Waals heterostructures.

This thesis will go over the properties of the quantum Hall effect that is seen in graphene, but incorporated with a SOC material, molybdenum disulfide, by using highly sensitive capacitance measurements. Chapter 2 will discuss the theory of Hall effect and its analogues, quantum capacitance and the density of states, and the various materials that are used. The process that is used to fabricate devices for the capacitance measurements will be found in Chapter 3. Then, in Chapter 4 the measurement techniques are outlined, including which instrumentation is used. The results are detailed in Chapter 5. Lastly, possible improvements and plans for future research are discussed in Chapter 6.

Chapter 2

Theoretical Background

This chapter reviews the theoretical background required to understand the experimental procedures and measurements performed, beginning with an overview of the Hall effect and its quantum analogues. It then goes on to describe classical and quantum capacitance and the differences between them. Lastly, it will cover the theoretical band structures for the materials used in these experiments.

2.1 The Hall Effects

2.1.1 Hall Effect

In a sheet of metal or semiconductor placed in a perpendicular magnetic field, one can apply a current and find there is a voltage difference across the perpendicular axis. Figure 2.1 shows a schematic model of the effect that occurs when a magnetic field, \mathbf{B} , is applied to the sheet of metal in the z -direction. If a current is applied to the metal along the y -direction, a voltage manifests in the x -direction. This phenomenon was discovered in 1879 by Edwin Hall[24] and is aptly named the Hall effect. The Lorentz force acts on a charge carrier due to electric and/or magnetic fields, and it is responsible for deflecting the trajectory of charge carriers away from the y -direction[25]. The magnetic component can

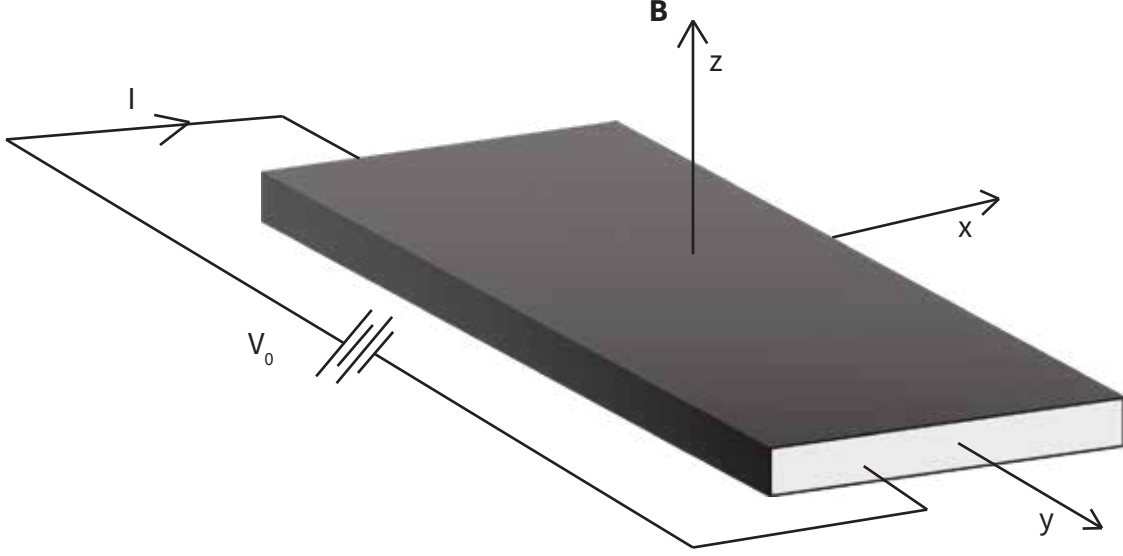


Figure 2.1: The Hall effect occurs when a voltage is measured in the x-direction while a current is applied in the y-direction. This happens under the condition that there is an applied magnetic field in the z-direction.

be written as:

$$\mathbf{F} = q\mathbf{v} \times \mathbf{B} \quad (2.1)$$

where q is a charge moving at velocity \mathbf{v} in the positive y-direction and \mathbf{B} is the magnetic field acting on those charges. This causes the negative and positive charge carriers to accumulate on opposite sides of the material, producing an electric field in the negative (positive) x-direction for positive (negative) q . The electric force from this built-in field will eventually even out the magnetic force giving:

$$q\mathbf{E} = q\mathbf{v} \times \mathbf{B}, \quad (2.2)$$

where \mathbf{E} is the electric field due to the build up of charge in the x-direction. The trajectory of electrons experiencing the Lorentz force can be visualized in Figure 2.2a. Continuing, we can use the equation for current density, $\mathbf{J} = ne\mathbf{v}$, to give us:

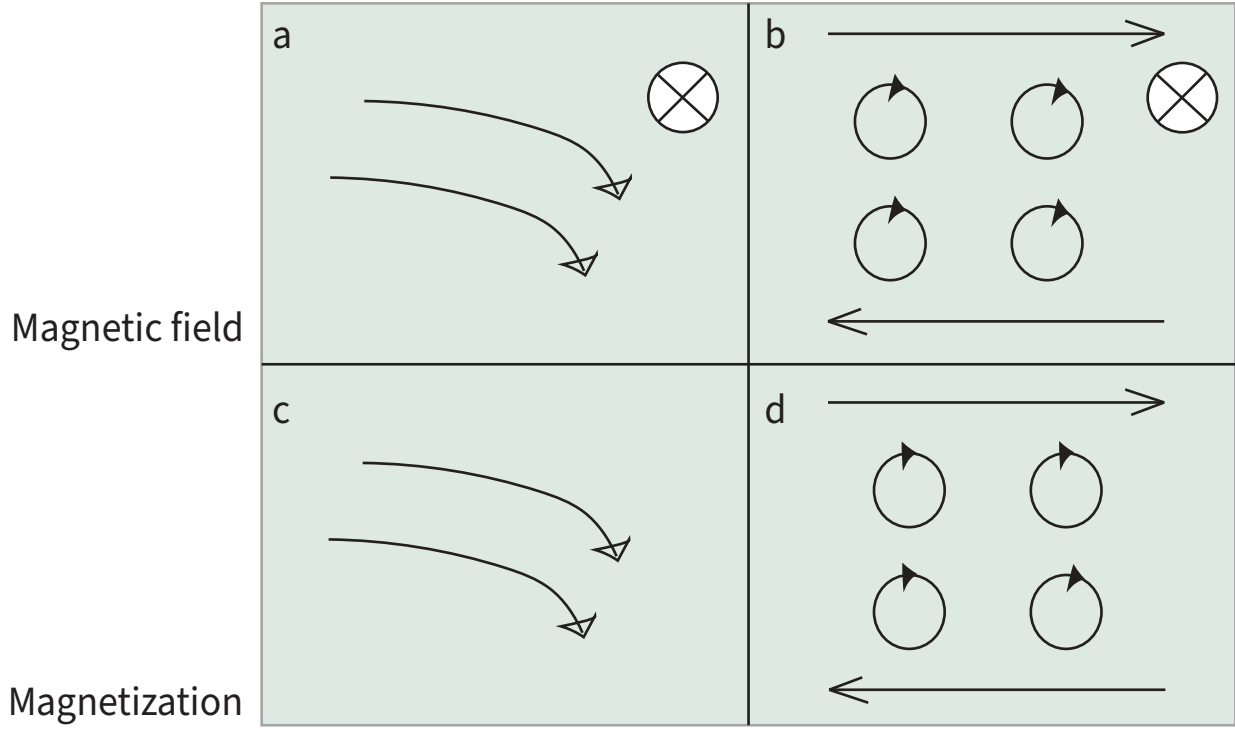


Figure 2.2: The Hall effect and 3 of its analogues. (a) The Hall effect: the Lorentz force acting on the electrons in the presence of a magnetic field going into the page. (b) The Quantum Hall effect: The electrons undergo skipping orbits at the boundaries and the other states are localized in cyclotron orbits within the middle. (c) Anomalous Hall effect: The material acts the same as the hall effect, except without an applied magnetic field. (d) Quantum Anomalous Hall effect: The quantum Hall effect without the presence of an external magnetic field.

$$E_x = -\frac{1}{ne}B_z J_y \quad (2.3)$$

which allows us to arrive at the well-known Hall coefficient:

$$R_H = \frac{E_x}{B_z J_y} = -\frac{1}{ne} \quad (2.4)$$

where n is the number of electrons and e is the charge of the electrons.

2.1.2 Quantum Hall Effect

In 1980, it was discovered that if the measurements for the Hall effect were tested under helium temperatures (4K) in a silicon field effect transistor subjected to a magnetic field of 15 T[10], the values of the Hall conductance became quantized at values of e^2/h and the longitudinal resistance dropped to zero. Figure 2.2(b) shows a model representation of the electronic states in a device exhibiting the quantum Hall effect (QHE). Here, skipping orbits at the edges of the sample result in dissipationless edge states and closed cyclotron orbits in the bulk of the sample produce insulating behavior. This picture is representative of the situation when the Fermi energy of the material lies between two Landau levels, whose energies are quantized to

$$E_n = \left(n + \frac{1}{2}\right) \hbar\omega_c \quad (2.5)$$

with n being an integer and ω_c is the frequency from the cyclotron orbit.

2.1.3 Anomalous Hall Effect

In ferromagnetic materials, it was realized that the Hall voltage was 10 times larger than in a nonmagnetic conductor. This discovery by Edwin Hall in 1881 was later dubbed the anomalous Hall effect (AHE). It has the same electrical response as the Hall effect, except without the presence of an external magnetic field. The Hall resistance for the magnetic material has two components: one that is proportional to the applied magnetic field and one that is proportional to the magnetization [26]. The latter is the anomalous contribution. The Hall resistance can then be written as:

$$R_{xy} = r_0 H + r_\alpha M, \quad (2.6)$$

where M is the magnetization of the sample, H is the applied magnetic field, and r_0 and r_α relate to the strength of the resistivities. Whereas the Hall resistivity r_0 depends on carrier

density, the anomalous resistivity r_α depends on a variety of material specific parameters[27]. Since the material itself is magnetic, it intrinsically breaks time reversal symmetry, a necessary ingredient for the Hall effect. Other factors that are responsible for this effect include spin orbit coupling and disorder effects. Panel c of figure 2.2 shows a visualization of the anomalous Hall effect.

2.1.4 Quantum Anomalous Hall Effect

It is logical then to wonder if the anomalous Hall effect can be quantized in the same sense as Hall effect. It has been shown that there is a quantum anomalous Hall (QAH) effect when time reversal symmetry is broken[12]. This requires the material to be a ferromagnetic semiconductor. The material has edge states with theoretically dissipationless currents called chiral edge channels. A QAH insulator is synonymous with a Chern insulator, meaning that it is a 2-dimensional insulator that has broken time-reversal symmetry. The chiral edge states are a characteristic of Chern insulators and are given by the Chern number.

2.2 Capacitance

To get an elementary idea of capacitors and measurements of capacitance, it is easiest to start with parallel plate capacitors. By connecting these plates to a battery and applying a potential difference, V , equal but opposite charge, q , will build on each of the plates. The charge and applied voltage are related in the following way:

$$q \equiv CV \tag{2.7}$$

where C is the capacitance. It is determined by the geometry of the plates of the capacitor and the dielectric that separates them ($C = A\epsilon/d$).

Capacitance measurements can be performed in different ways. A simple meter can

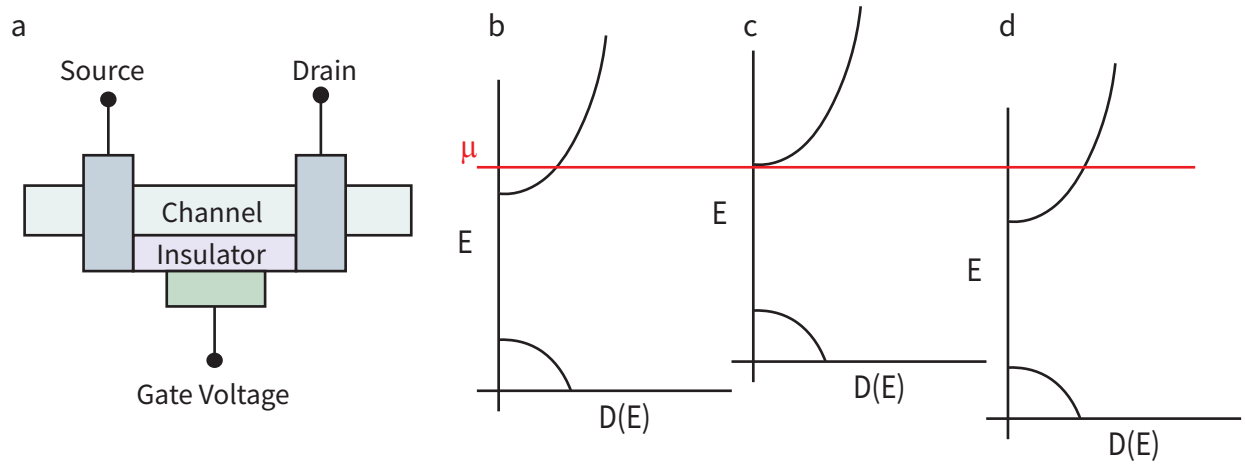


Figure 2.3: (a) Example of a device used for capacitance measurements. Labeled are the source and the drain to the device, the material being probed or the channel, an insulating material, and a gate voltage applied to the bottom. (b-c) Plots of the density of states of a two band semiconductor for different gate voltages. The red line, μ , indicates the electrostatic chemical potential. (b) The density of states with no gate voltage. (c) When a negative voltage is applied to the device. The conduction band will move to be in line with μ . (d) When Fermi level is moved inside the the conduction band, the material becomes conducting.

measure capacitance by sending a known current through the device under testing (DUT) and measuring the rate at which the voltage rises. A fast rate of change in the voltage correlates to a smaller capacitance. This can be seen by rearranging equation 2.7 to $C = q/V$. The next method of measuring a capacitor is to pass a high frequency alternating current through the DUT and measure the voltage change across it. This is similar to the first method, but measured over several cycles of charging and discharging. The last and most precise way is to test capacitance by using a capacitance bridge. In this method, the DUT is placed in a circuit with a known capacitor. The capacitors are each paired with a resistor and the signal across them is changed until the circuit is balanced. The unknown capacitance can then be determined.

A majority of semiconductor devices are layered with a dielectric to isolate the gates from the channel. The capacitance of these devices is then the sum of the geometric capacitance from the dielectric and the quantum capacitance from adding carriers in the band structure of the semiconductor[21]. For devices with large density of states (DOS), the capacitance is just that of the geometric capacitance. On the other hand in low dimensional system, the effects of quantum capacitance outweigh that of the geometric capacitance because of the low DOS. Quantum capacitance is proportional to the density of states and can show us more subtle information about the system, like the band structure.

To show how the quantum capacitance is related to the density of states, we introduce the quantum capacitance of a simple two band semiconductor transistor (figure 2.3). Figure 2.3(a) shows a model of a device made with a semiconducting channel material. Figure 2.3(b-d) shows plots of the density of states for this semiconductor. The red line, μ , is the electrochemical potential. This is the level up to which the states are filled. When adding a negative gate voltage to the device shown in figure 2.3(a), the energy levels will float up, so that the electrostatic potential is right at the conduction band. To find the number of electrons, we can use the following equation[28]:

$$N = \int_{-\infty}^{\infty} dE D(E - U) f_0(E), \quad (2.8)$$

where $D(E)$ is how many electronic states there are at energy level E and f_0 is the fraction that are filled. With a transformation of variables, we arrive at the more useful equation:

$$N = \int_{-\infty}^{\infty} dE D(E) f_0(E + U). \quad (2.9)$$

When the electrostatic potential is inside the conduction band, figure 2.3(b), we can find the quantum capacitance of the device by calculating how the number of charged particles, N , changes with a small change in the channel potential, U . We can start by taking the derivative of equation 2.9 with respect to the chemical potential.

$$\frac{dN}{dU} = \int_{-\infty}^{\infty} dE D(E) \frac{\partial f_0(E + U)}{\partial E}. \quad (2.10)$$

This quantity will be negative because of the Fermi function and it will give the average density of states, D_0 .

$$\frac{dN}{dU} \equiv -D_0. \quad (2.11)$$

Here, $-D_0$ is the average density of states in the energy range of interest. If we go on to find the change in the charge due to the change in the potential, we find that it is equal to the quantum capacitance,

$$\frac{d(qN)}{d(\frac{U}{-q})} = q^2 D_0 \equiv C_Q, \quad (2.12)$$

or

$$\frac{dN}{dU} = -D_0 \equiv \frac{-C_Q}{q^2}. \quad (2.13)$$

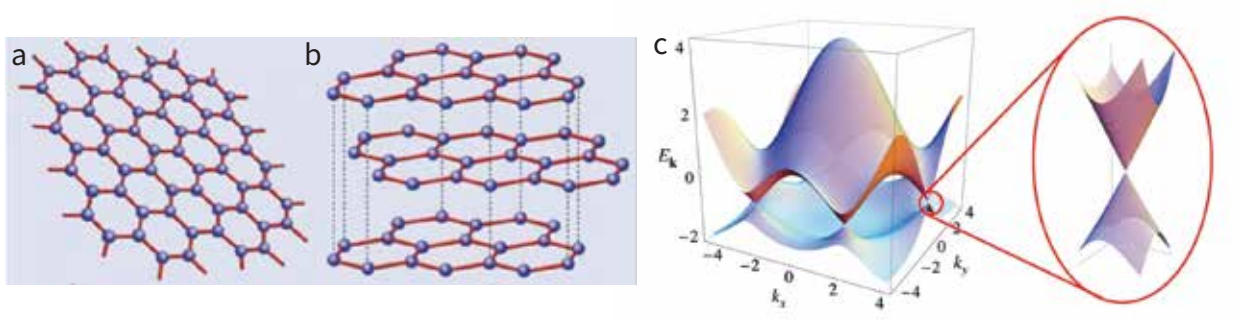


Figure 2.4: Graphene crystal structure and energy band structure. Figure adapted from Castro Neto et al. [2]. (a) The crystal structure for monolayer graphene. It is a honeycomb lattice made up of carbon atoms. (b) The crystal structure for multiple layers of graphite is monolayer graphene stacked on top of itself. (c) Graphene's band structure with hopping values of $t = 2.7eV$ and $t' = -0.2t$. The inset shows a zoomed in picture of one of the Dirac cones.

This shows us that by measuring small changes of the quantum capacitance, we get a picture of the density of states of the material.

2.3 Material Theory

We now move to a more general discussion of the theoretical properties of the materials of interest in our work. We start with graphene, a single layer of graphite, continue with molybdenum disulfide (MoS_2), a transition metal dichalcogenide, and finish with boron nitride (BN).

2.3.1 Graphene

Graphene has been a material of interest since its discovery in the condensed matter field[29]. Graphene is a 2-dimensional system notable for its high electron mobility, meaning that the electrons can flow easily through the material, making quantum effects easily distinguishable. Capacitance measurements are ideal for graphene because of the ability to easily tune the electrical properties with an electrostatic gate. In 2004, it was

found that graphite can be exfoliated down to a single layer of atoms by using the scotch tape method [16]. There are 3 thicknesses of few-layer graphene that are of interest to us: monolayer, bilayer, and trilayer.

For monolayer graphene, the electronic band structure can be calculated from a tight-binding Hamiltonian [2]:

$$H = -t \sum_{\langle i,j \rangle, \sigma} (a_{\sigma,i}^\dagger b_{\sigma,j} + H.c.) - t' \sum_{\langle\langle i,j \rangle\rangle, \sigma} (a_{\sigma,i}^\dagger a_{\sigma,j} + b_{\sigma,i}^\dagger b_{\sigma,j} + H.c.), \quad (2.14)$$

where $a_{i,\sigma}$ and $a_{\sigma,i}^\dagger$ are the annihilation and creation operators with spin, $\sigma = \uparrow, \downarrow$. This Hamiltonian will produce the following energy bands [30]:

$$E_{\pm} = \pm t \sqrt{3 + f(\mathbf{k})} - t' f(\mathbf{k}), \quad (2.15)$$

where

$$f(\mathbf{k}) = 2 \cos(\sqrt{3}k_y a) + 4 \cos\left(\frac{\sqrt{3}}{2}k_y a\right) \cos\left(\frac{3}{2}k_x a\right). \quad (2.16)$$

In equation 2.15, the plus sign represents the upper band and the minus sign represents the lower band. If $t' = 0$, we can see that it is symmetric around zero energy, but with a finite t' the bands become asymmetric because of the electron-hole symmetry being broken.

Figure 2.4(c) shows the energy spectrum with finite t and t' and the inset of the figure shows one of the Dirac cones.

To observe quantum anomalous hall effect, a material needs to have intrinsic magnetism and a strong spin orbit energy. Unfortunately graphene has neither of these properties intrinsically and so we look to other materials, such as MoS₂ with strong spin orbit coupling.

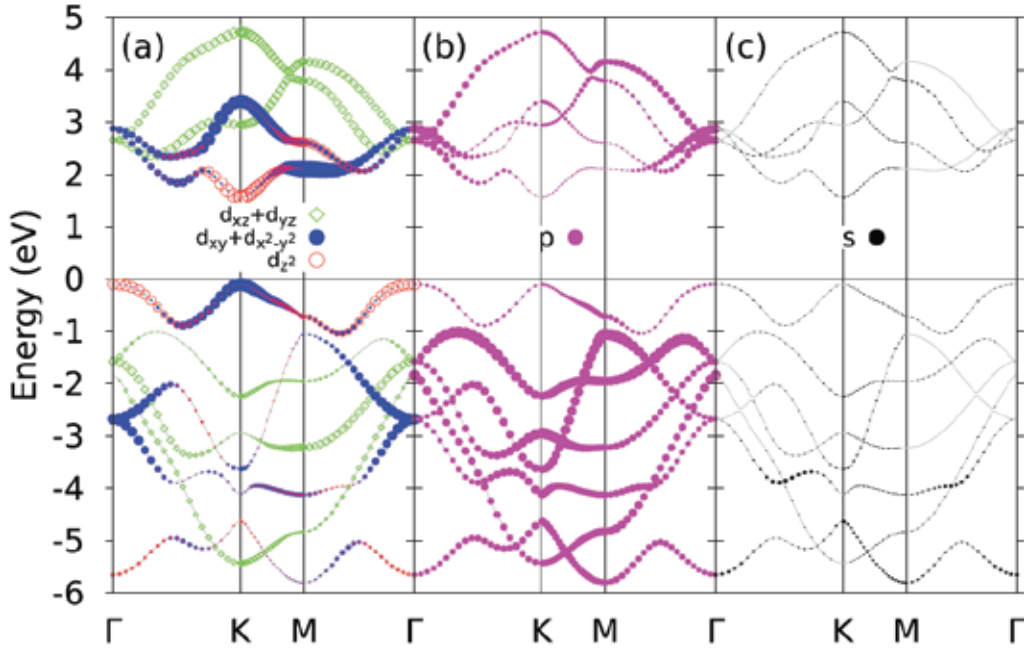


Figure 2.5: The theoretical band structure of MoS₂, calculated from first principles. This figure is adapted from [3]. (a) The *d* orbital contribution. (b) The *p* orbital contribution. (c) The *s* orbital contribution.

2.3.2 Molybdenum Disulfide

Recently, transition metal dichalcogenides (TMDCs) have been studied for use in electronics and opto-electronics [31]. Molybdenum disulfide (MoS₂) is one of these TMDCs. A monolayer of MoS₂ consists of a single layer of molybdenum that is sandwiched between two sulfur layers. Graphene is similar to MoS₂ in the sense that the conduction and valence bands are located at the first Brillouin zone at the K and -K points [3]. MoS₂ differs from graphene in several ways. It is a semiconductor, whereas graphene has no band gap. The second main difference is that MoS₂ has a strong spin-orbit coupling from its heavy metal atoms [32].

Figure 2.5 shows the calculated band structure for MoS₂ from first principles and the separate contributions from the *d*, *p*, and *s* orbitals [3]. It can be seen that MoS₂ is a semiconducting material with a band gap of approximately 1.8 eV.

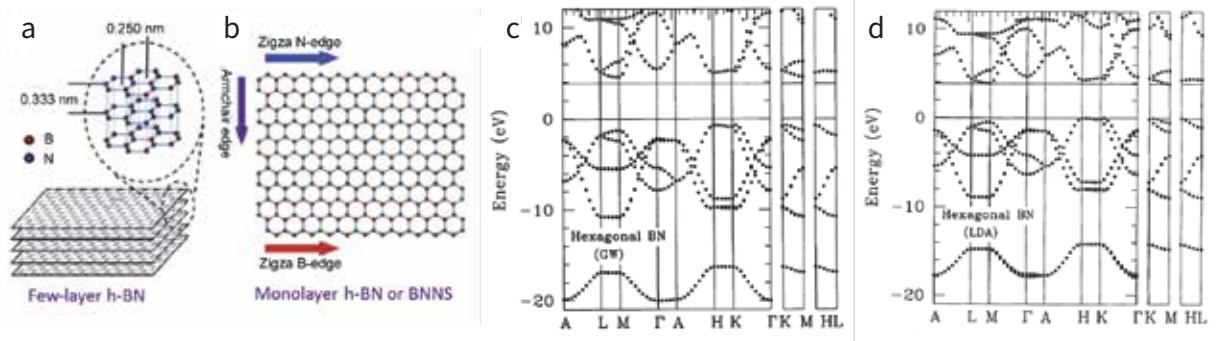


Figure 2.6: The crystal structure[4] and the band structure[5] of hBN. (a) Multi-layer BN is similar to graphite in that the bulk structure is composed of monolayers stacked on top of one another. (b) Monolayer BN has the same hexagonal or honeycomb structure as graphene. (c) The LDA (local density approximation) band structure of bulk hBN. (d) The GW (Coulomb-Green's function approximation) band structure of bulk hBN.

2.3.3 Hexagonal Boron Nitride

Hexagonal boron nitride (hBN) has an atomically smooth surface and it has interatomic spacing close to that of graphene, but has a large band gap in comparison to graphene [4]. This makes it an ideal candidate as an insulating layer in our devices. hBN has a honeycomb lattice and has alternating boron and nitrogen atoms. The crystal structure of hBN can be seen in figure 2.6(a-b).

Figure 2.6(c-d) show the band structure of bulk hBN. The local density approximation (LDA), shows that hBN has a band gap of 3.9 eV, making it a wide-band gap semiconductor[5] but effectively insulating in our experiments.

Chapter 3

Fabrication Processes for Capacitance Devices

This chapter discusses the different materials and techniques used to fabricate the devices used to make capacitance measurements. These materials include graphite, hexagonal boron nitride (hBN), and molybdenum disulfide (MoS_2). The chapter begins with stack design, the process we use to design our heterostructure stacks before creation. This section includes descriptions of the exfoliation of the materials and our stacking technique used to combine the individual materials into a complete stack. The chapter continues with photolithography, a process that allows us to create micron-sized patterns on the surface of our heterostructures for the purpose of etching and to create electrical contacts. The chapter concludes with a discussion of our etching process that allows us to etch away unwanted portions of the heterostructures.

3.1 Stack Design

Summarizing the stack design, the materials we exfoliate are used to design the devices. The stacks are designed to have a relatively large, $20\text{ }\mu\text{m}$ by $20\text{ }\mu\text{m}$, overlap area with limited amount of extra overlap of the materials. It is necessary to only have the

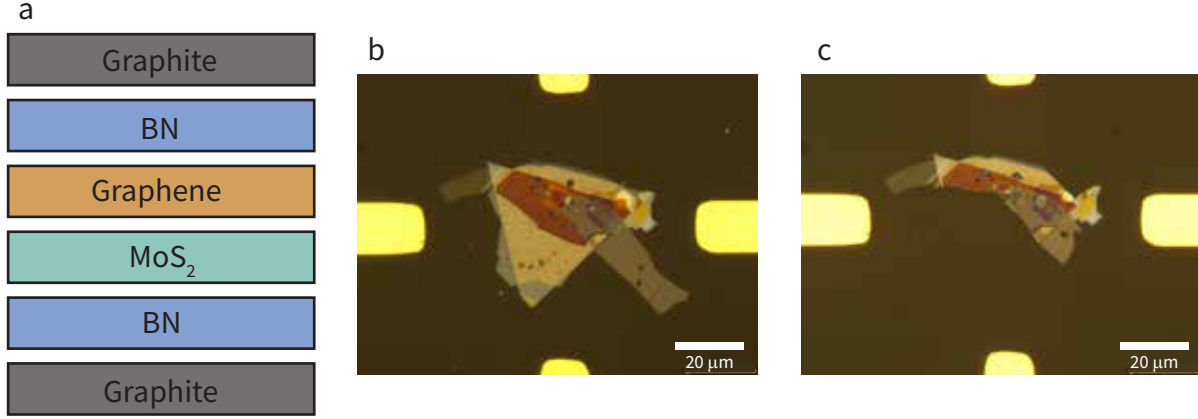


Figure 3.1: Overview of the stack design and etching. (a) A model of a representative heterostructure. There are two graphite gates on the top and the bottom of the stack. There is then an insulating layer of material next to the gates, with the graphene and MoS_2 in the middle. (b) An optical image of a stack before the etching process. (c) An optical image of the same stack after the excess material has been etched away.

materials overlap in the same area. Extra overlap of the graphite gates without graphene in between, for instance, will result in a capacitance signal derived only from the gates themselves and not the material of interest between the gates. Figure 3.1(a) shows a model of a heterostructure stack and the order, starting from the top layer, of the stacks. The outside is sandwiched with graphite, while there is a layer of BN insulating the graphene and MoS_2 in the middle. The graphite layer is first picked up with a large BN flake (not shown). Subsequent flakes are picked up in the same order, from top to bottom, until the entire stack is complete. Figures 3.1(b) and 3.1(c) show optical images of a completed stack that was used for measurements described in later chapters. The middle panel shows the stack before the excess overlap was etched away and right panel shows the stack after the etching process.

3.1.1 Exfoliation

After we have a design for which materials we would like to use and how we will stack them, we can start looking for the materials that we will use. The materials are exfoliated

onto a 500 μm thick silicon (Si) chip with a 300 nm layer of silicon dioxide (SiO_2). The chips are made by dicing a 4 inch wafer into 10 mm squares with a diamond tipped scribe. The material is exfoliated by using the scotch tape method [16, 33]. The basic process for exfoliating the materials is the same, but some small variations in the process are utilized to increase the yield of high quality flakes. When exfoliating BN, a few small bulk pieces are placed on the tape. When exfoliating other material, the tape is pressed on small millimeter sized pieces. The tape is then adhered to itself and pulled apart until there is what looks to be an even layer of material on the tape. We call this the parent tape. Another piece of tape is then taken and adhered to the parent tape and pulled off. This is the daughter tape. The daughter tape is then placed on to the Si/ SiO_2 chips. When exfoliating BN, the tape is pressed down firmly with a finger tip for approximately 10 seconds before being pulled off slowly. When exfoliating graphite and MoS_2 , the tape is flattened with the backside of a razor blade and then slowly pulled off. The different methods used for these materials are due to the structures of the materials. Graphite and MoS_2 have a lower cleavage energy and more malleable character when compared to BN, leaving thinner flakes of material. The chips with the material are then scanned with an optical microscope under white light illumination. Images are taken of flakes of material for potential stacks. Figure 3.2 shows several optical images of flakes used to make the first few layers of the model heterostructure in panel d. Flakes are chosen based on their thickness and surface area. The thickness of the flakes can be determined by using image contrast comparisons[34, 35, 36]. To perform a contrast comparison, the image is first loaded into imaging software (Gwyddion). Using the software, a contrast profile can be taken across the flake, showing the contrast difference between the background (Si/ SiO_2) and the flake itself. The contrast difference can be compared with values reported in literature to determine the flakes thickness[34]. This method is reliable for mono and few layer flakes but becomes unreliable for several layers. The general color of the flakes can also be used as a guide to the approximate thickness. For instance, the graphite flake in

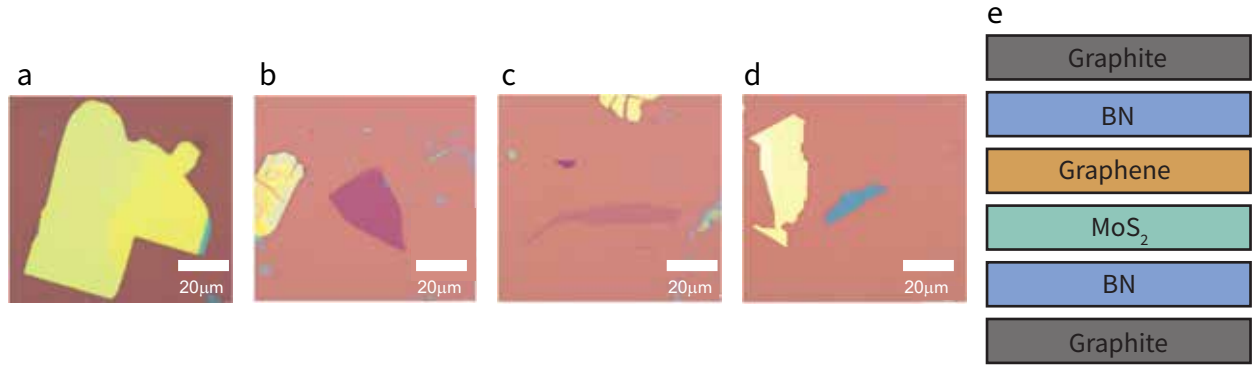


Figure 3.2: Optical microscopy images of various flakes of materials that have been exfoliated using the Scotch tape method. These include: (a) Flake of BN that is used as the first pick up layer due to the large surface area. BN is also used as an insulating layer in between stack. (b) Flake of graphite that was used as a top gate. The graphite that is used for gates is typically > 5 layers. (c) Flake of bilayer graphene (d) Flake of MoS₂. MoS₂ is used with graphene due to its larger spin orbit coupling energy.

panel b of Figure 3.2 is purple and can be approximated as having a thickness of 5 - 10 layers. This thickness is suitable for a top or bottom gate.

3.1.2 Stacking

Once we have the stack designed and the different flakes that we want to use ready, we can begin the stacking process. Traditionally, this method was done using a polypropylene carbonate (PPC) film to pick up the different layers of the stack[37, 38]. Recently, our lab has developed a stacking process using common household nail polish[39]. Not only is this process more cost effective, but it is less complicated and leaves us with high quality stacks.

To stack these materials using nail polish we start with a glass microscope slide. A cylindrical piece of polydimethylsiloxane (PDMS) is stamped out of a thick film (5 mm thick) using a biopsy punch that is about 3 mm in diameter and placed towards one end of the glass slide. A piece of clear Scotch tape is placed over the PDMS in order to create a raised area that we refer to as a hemisphere. We then place a drop of Revlon clear nail polish on the center of the hemisphere using a toothpick. The glass slide is then placed on

a hot plate at 90°C for approximately 1 minute to cure and harden the nail polish.

This glass slide is then loaded into a micromanipulator with the hemisphere side facing down. The micromanipulator is positioned over a stage under an optical microscope. A model representation of this can be seen in figure 3.3(a). A Si/SiSO₂ chip with a flake of interest on it is placed on the center of the stage. The micromanipulator is then used to lower the glass slide over the "chosen" flake until the nail polish touches down on the Si/SiSO₂ chip. Figure 3.3(a-c) shows this process for the first BN pick up. After the slide pins part of the BN with the nail polish, it is slightly lowered until the nail polish envelops the whole flake of BN. The slide then can be brought back up quickly, with a popping motion. The adhesion force from the nail polish is enough to pick up the first BN and it is strong enough to undergo the abrupt motion. For subsequent flakes, van der Waals forces between the other materials are used to pick them up. The process to find the flake is repeated (figure 3.3(d)). The difference comes in when needing to pick up the flake. The stage has a heater that is initially set at 40°C. Once the flake is pinned on a corner with the BN on the nail polish, the heater is slowly raised 2°C at a time (figure 3.3(e)). The contact between the nail polish and the surface will slowly grow and envelope the flake. The temperature increase is stopped once the flake is fully covered by the nail polish. This usually happens around 50°C-60°C. The temperature is then held there for about 1 minute until it is reset to its starting point of 40°C. When the temperature is reset, it slowly comes down, causing the contact to shrink and pull up the flake as seen in figure 3.3(f). This process is repeated until all flakes are stacked on the nail polish hemisphere.

The next step in this processes is to transfer the stack to a chip made of either quartz or undoped silicon. These materials are used because they are insulators and will not contribute to stray capacitance during the measurements. The chips have an outer ring of electrode pads prepatterened out of gold. The chip is placed on the stage. The glass slide is positioned using the micromanipulator in order to transfer the stack to the center of the chip. The heat of the stage is set to 40°C. The slide is slowly lowered down onto the chip

until part of the stack is pinned in between the nail polish and the chip. The heat is increased by 20°C and held at the that temperature for about 5 minutes. The nail polish will start to spread out and cover the stack. The z-axis control on the micromanipulator is used in order to keep the whole chip from laminating. This process is repeated again, so that the temperature is at 80°C. From here, the stack can be squeezed.

The squeezing process will help push the bubbles containing water and adsorbates out from in between layers, creating a better contact. To squeeze the stack, the z-axis of the micromanipulator is used to pull up the stack and push it back down, always keeping one part of the stack pinned. After the stack is squeezed, the temperature is brought up again by 20°C at a time. After each temperature raise, the temperature is held for about 5 minutes. This process repeats until the temperature reaches 110°C, melting the nail polish completely. The temperature is held here while the z-axis is slowly brought up. The glass slide is pulled up until the nail polish detaches from the chip. The chip is placed in a bath of acetone for about 10 minutes or until all of the nail polish is removed. This chip is rinsed with IPA and dried carefully with a nitrogen gun.

3.2 Photolithography

After the stack has been transferred to the chip with the gold pre-electrode pattern, the stack then undergoes a photolithography process in order to create a mask to etch the stack and then later pattern electrodes to each layer. This process is performed at the UNLV Nanotechnology Center, a class 1000 cleanroom located in the Science and Engineering Building.

First we design a pattern for the etch mask in CAD software. The design of the mask for the stack is made to maximize device area while etching away any unwanted overlap of materials. The pattern of the mask is then loaded into the photolithography software.

For patterning the mask, two different recipes were tested. The monolayer recipe

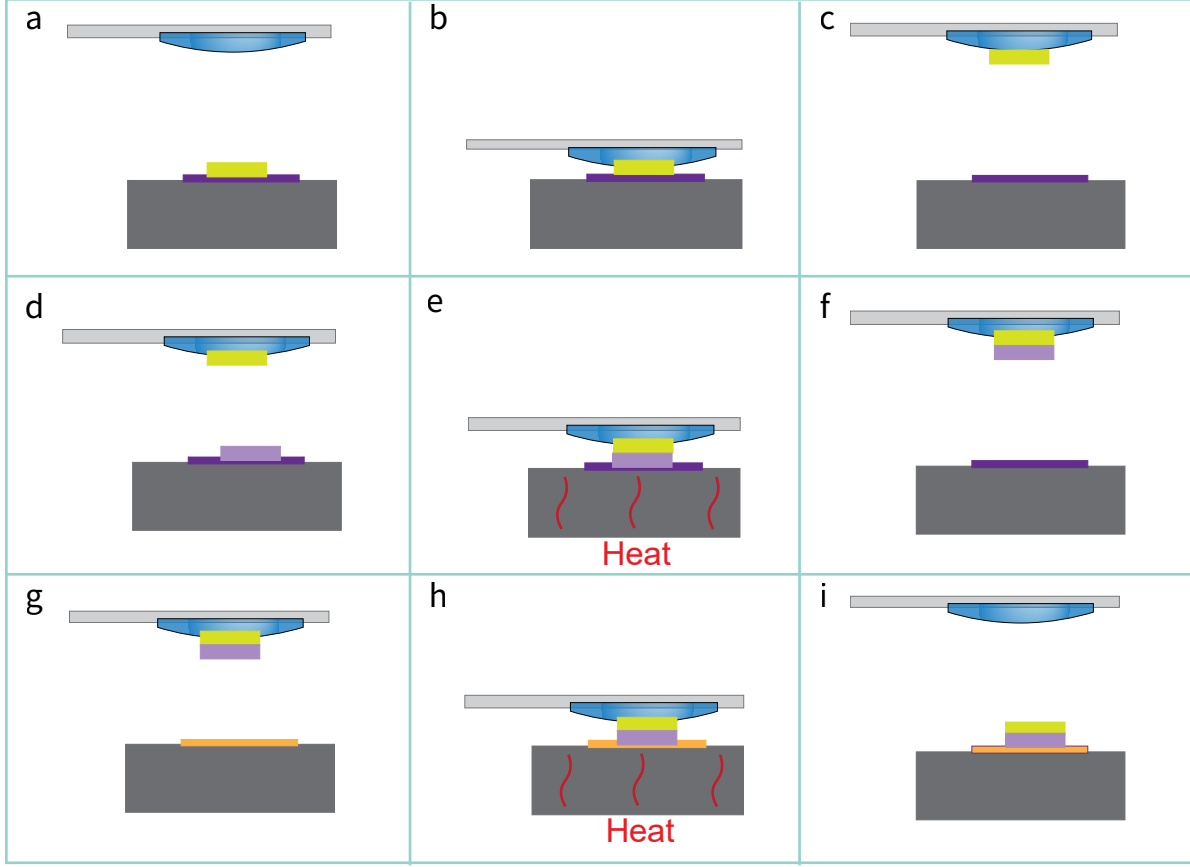


Figure 3.3: Overview of the stacking process that is used to fabricate the devices that we use for capacitance measurements. The first row of figures shows how the first piece of BN is picked up using adhesion forces from household nail polish. The second row of panels shows how later flakes are stacked using the van der Waals forces between the materials. The last row of images is how the stack is transferred to a substrate of choice. (a) At the top is the glass slide with the hemisphere, in blue, that is created by layering a piece of clear tape over a cylinder of PDMS. A drop of nail polish is then put on the top of the hemisphere. At the bottom shows a flake of BN that has been found on top of a Si/SiO₂ chip. (b) The glass slide is slowly lowered over top of the flake using the z-axis on the micromanipulator. The nail polish drop then pins a corner of a flake of material and is continuously brought down until the flake has been covered. (c) The slide is pulled up quickly, taking the flake of material with it. (d) The slide with the BN is positioned over the next flake of material. (e) The slide is slowly lowered pinning a corner of a flake of material with the BN. Heat is applied from the stage in increments of 2°C until the flake is covered by the BN and nail polish. This happens around 48°C. (f) The heat is then lowered back to 40°C and the z-axis is used to slowly bring up the picked up flake. The materials should now be stacked on top of each other. (g) To transfer the whole stack, the slide is positioned in reference to the electrode position on the chip that the stack will be transferred to. (h) The slide is lowered and a corner of the stack is pinned to the substrate. The heat is raised in increments of 20°C. The z-axis is used to keep the nail polish from laminating the while chip and keeping the nail polish to the area around the stack. The heat is stopped once it reaches 110°C. (i) The heat is held at 110°C while the z-axis is used to slowly pull up the glass slide.

consisted of only spinning photoresist on to the chip. This recipe was found to be best when depositing the 80 nm chromium (Cr)/gold (Au) electrodes. When depositing copper (100 nm), the excess copper would not cleanly lift off and leave the copper mask behind for etching. A bilayer recipe was developed to overcome this difficulty. This recipe involves spinning a layer of lift off resist (LOR) before spinning a layer of photoresist on to the sample. After the pattern has been exposed, the developer will dissolve the LOR slightly faster than it does the photoresist. This will leave an undercut under the photoresist layer, which helps with the removal of the excess copper.

To prepare the sample for photolithography with the bilayer recipe, the chip with the stack on it is placed on a spinner and held by a vacuum. First, LOR is dropped on the chip with a pipette and is let to sit for 1 minute to promote adhesion. Then the LOR is spun on the chip for 30 seconds at 2000 RPM. The chip with the LOR is transferred to a hot plate at 190°C for 5 minutes. The chip is then returned to the spinner and photoresist is dropped onto the chip. The photoresist is then spun on the chip for 30 seconds at 4000 RPM. The chip is transferred to the hot plate at 95°C for 60 seconds. These spinning recipes result in a layer of LOR with a thickness of approximately 300 nm and a layer of photoresist with a thickness of about 1 micron.

The chip is placed on a stage of a Microlight 3D Smart Print. The Smart Print allows us to use lithography techniques with a digital mask pattern as opposed to a hard mask. This allows us to expose custom patterns onto any device without the need to first create a hard mask. This is very convenient when designing electrodes or masks for etching. The smallest resolution that we can achieve is $2\text{ }\mu\text{m}$. The exposure time and objective size is chosen depending on what material the chip is and how big the pattern is. For a quartz chip, slightly longer exposure times are used compared to a Si/SiO₂ chip. The difference in exposure times is due to the opacity of the material. The different exposure times can be seen in table 3.1 and 3.2. The 10x objective size is used to make the pattern for the etch mask. The pattern is lined up to the stack and exposed. The chip is placed in developer

and lightly swirled for 60 seconds to remove the photoresist and LOR that was exposed with the Smart Print. The UV light from the Smart Print breaks the polymer bonds in the LOR and resist so that the developer can remove the material from the pattern areas.

Table 3.1: Exposure times when doing a monolayer photoresist mask

Objective	Substrate	Exposure time [s]
10x	Si/SiO ₂	0.8
2.5x	Si/SiO ₂	3.7-3.8
2.5x	Quartz	4.5

Table 3.2: Exposure times when doing a bilayer LOR/photoresist mask

Objective	Substrate	Exposure time [s]
10x	Si/SiO ₂	1.4
10x	Quartz	1.5
2.5x	Si/SiO ₂	3.5

For an etch mask we use copper which is deposited to the chip surface using a benchtop sputter system. The thickness of the copper layer is approximately 100 nm. The chip is then placed in resist remover to lift off the unwanted copper. This will leave only the pattern with the copper layer and the unwanted parts of the stack exposed for etching. The etching process will be discussed in detail in the next section: 3.3.

After the etching process, the chips go through the photolithography process again to deposit and create electrical contacts to the stack layers. This time a single layer photoresist mask recipe is used. The single layer recipe works best for the Cr/Au electrode deposition without wasting excess lithography materials. Photoresist is spun on the chip for 30 seconds at 4000 RPM. The chip is placed on a hot plate at 95°C for 60 seconds. The chip is then placed on the Smart Print stage and aligned to expose an electrode pattern that connects the larger outer pads to the stack. The chip is then placed in developer and swirled for 60 seconds. Figure 3.4(a) shows an example of the chip after the electrode

pattern has been created. The brown areas in the image show the chip surface and the green areas show the resist. The heterostructure is located in the middle of the image. Three electrodes have been patterned for this stack. One for each of the gate electrodes and one to contact the middle layer of graphene and MoS₂. The stack is then placed in an electron beam deposition chamber. 10 nm of chromium is deposited and then an 80 nm layer of gold is deposited on top of the chromium. Figure 3.4(c) shows the stack after the electrodes have been deposited and the unwanted gold has been removed. Now, the brown regions are the substrate surface and the gold regions are the electrodes. Figure 3.4(d) shows a lower magnification image of the same stack showing the connections made to the larger prepatterned electrodes.

3.3 Etching

This is a critical step for the capacitance devices, and so we have devoted a separate section to this process which took several months to work out. Ideally when devices are fabricated, the materials are only overlapped in the same area. Unfortunately, it is unrealistic to line up the materials perfectly during the stacking procedure because all the flakes have different shapes. This causes the need to get rid of any unwanted overlap. After lithography and the copper mask has been deposited onto the stack, the stacks are etched in a plasma etcher. The stacks are etched by alternating gasses, O₂ and CHF₃, depending on what layers need to be removed. Table 3.3 shows the different etching parameters that are used. Figure 3.5 shows a stack after several etching steps. The first image (a) shows the stack before any processing has been done on it and the second image (b) shows the stack after the copper mask has been sputtered on it. For the stack design that is shown in section 3.1, these formulas are alternated, starting with the hBN formula. Figure 3.5(c) shows the stack after this first etch. After each trial of etching, the stack is viewed under an optical microscope to see which layers are left and judge which formula to use (figure

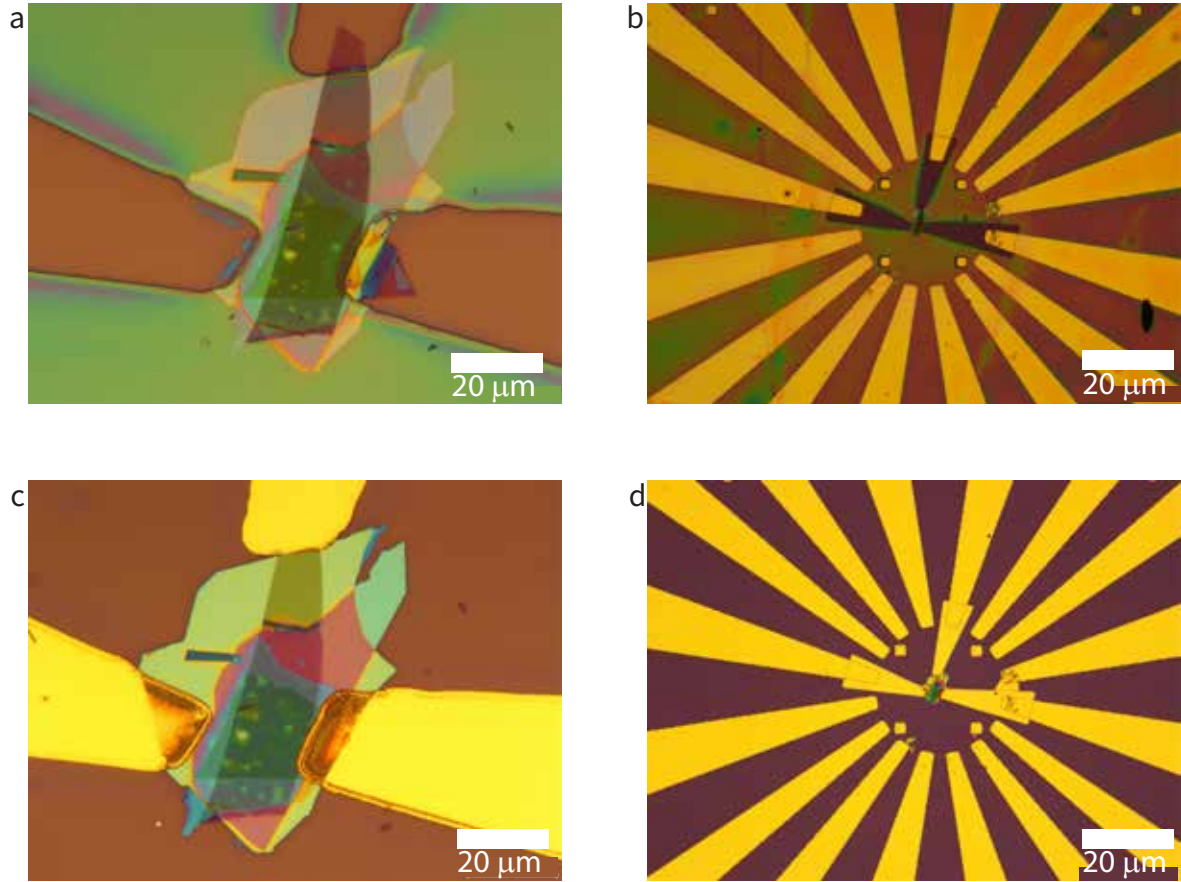


Figure 3.4: Optical images of a device after the photolithography processing and after gold electrodes have been deposited. (a-b) A mask is applied to the device using photolithography techniques. This mask is a single layer of photoresist. The brown regions are the exposed substrate surface after development and the green regions show where the resist still resides. (c-d) Gold is deposited to the chip using an electron beam deposition. The resist mask is removed using acetone and the gold electrodes are left where the photoresist was exposed.

3.5(d-i)). Once all of the material is removed that is not under the copper mask, the mask itself can be removed using an ammonium persulfate solution as seen in figure 3.5(j).

Table 3.3: Etch times depending on which material is being removed. Both of the recipes use 100 W of power.

Material	CHF ₃ [mL/min]	O ₂ [mL/min]	Time [s]
BN	50	50	15
Gr and MoS ₂	0	80	120

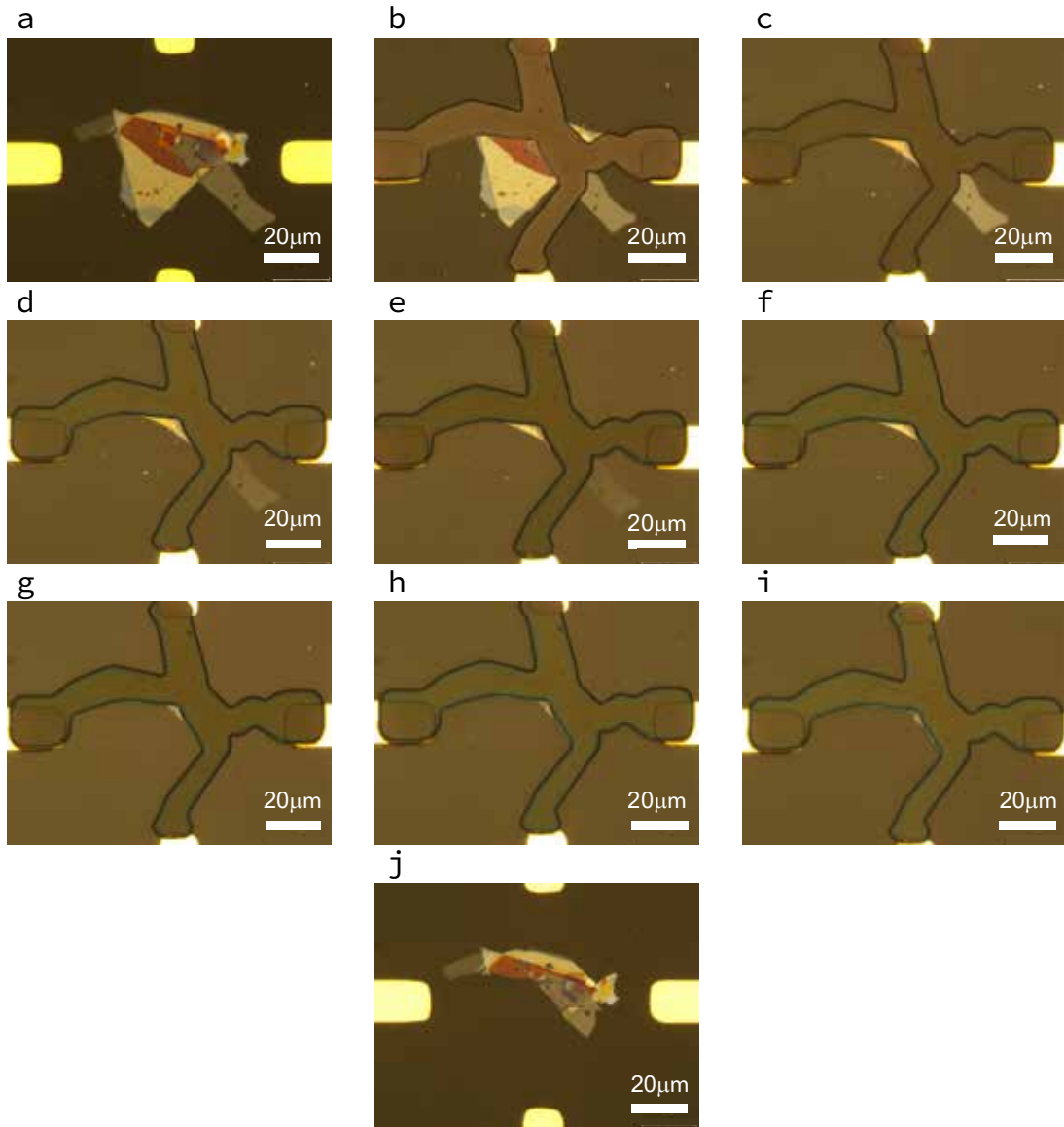


Figure 3.5: Optical images of a stack undergoing an etching process. (a) An optical image of the stack before the copper mask has been deposited. (b) The stack after the copper mask has been deposited, before etching has started. Images (c-i) are after different etching formulas for the different materials: (c) BN, (d) Gr, (e) BN, (f) Gr, (g) MoS₂, (h) BN, and (i) Gr. The last image (j) shows the stack after the copper mask has been removed.

Chapter 4

Instrumentation and Measurement

After the device has been patterned to electrodes, it is bonded to a capacitance bridge on a sample holder that will go into a cryostat (Quantum Design Physical Property Measurement System, PPMS). The capacitance bridge allows us to measure the small capacitance signals that are associated with our small micron-sized devices. Traditionally, capacitance bridges have been able to make measurements on devices that have a larger density of states (DOS). In the devices that we make, quantum capacitance outweighs the geometric capacitance due to their low DOS. With the setup that is described in this chapter, we are able to resolve attofarad (aF) quantum capacitance signals[40]. In this section, the setup for the capacitance bridge will be described, then the connections that are made from the capacitance bridge in the cryostat to the outside electronics will be reviewed, and lastly the actual measurement procedure will be discussed.

4.1 Instrumentation

4.1.1 Capacitance Bridge

The capacitance bridge setup will make highly sensitive capacitance measurements, on the order of attofarads (aF) at room temperature [40] [41] [42] [43]. We will also refer to it

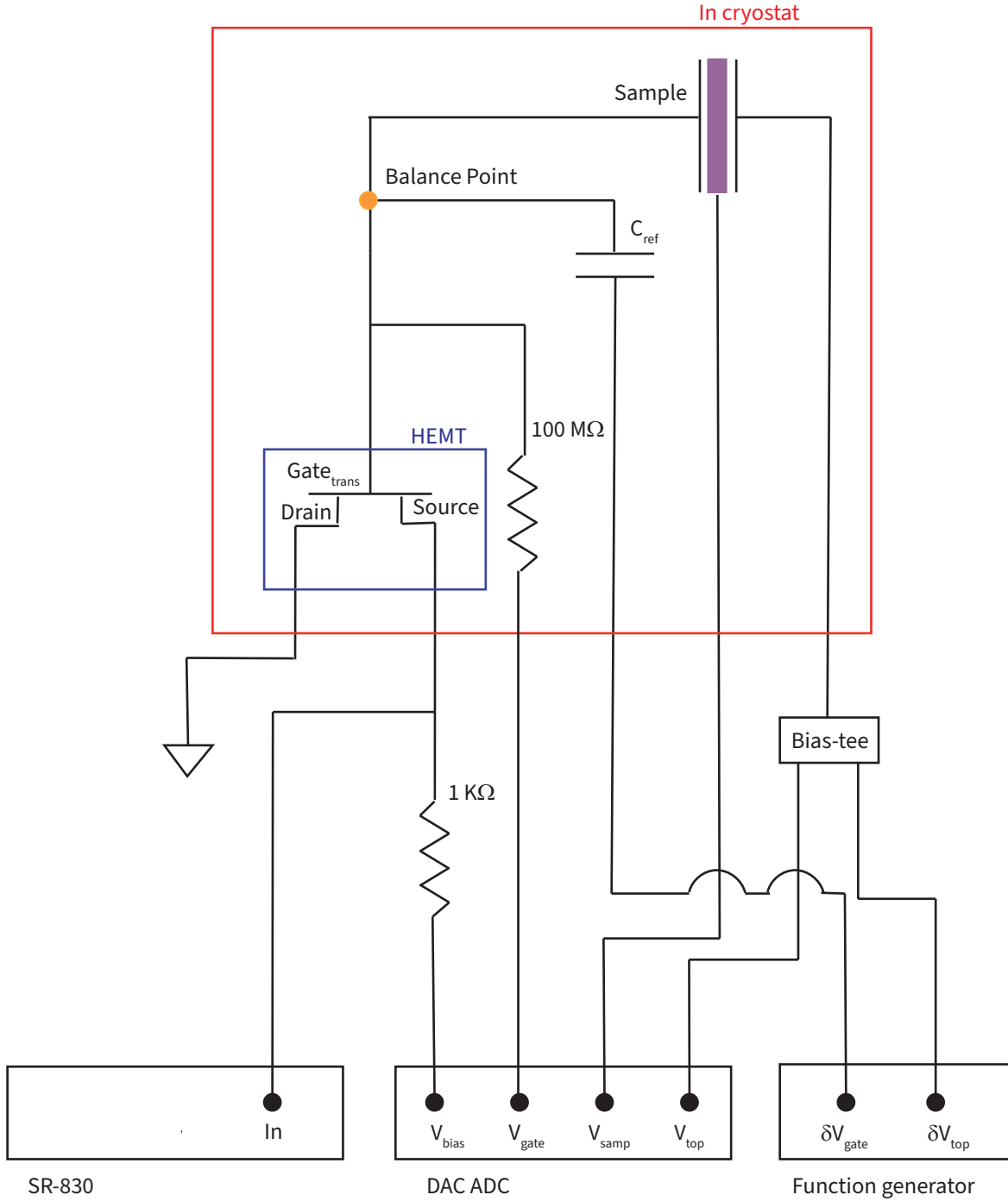


Figure 4.1: Schematic of the electrical setup used to make the capacitance measurements. The red outlined portion represents the electronics and device that are located inside the cryostat. See the main text for further descriptions.

as a transistor mount due to the geometry of the transistor on the capacitance bridge.

A traditional capacitance bridge circuit will have two capacitors, one with a known capacitance and one with an unknown capacitance. It will also have two resistors, where one or both are adjustable. These are all connected to what can be called a bridge point. An AC supply is applied to the circuit until the bridge point is balanced at zero voltage.

The capacitance bridge is connected to the device under test (DUT) and put into the cryostat. In figure 4.1, the electrical schematic of the capacitance bridge with the sample can be seen outlined in red. The sample is a triple layer capacitor made of two electrostatic gates and one middle layer. The purple line in the center of the sample (top right) represents the graphene. There is a voltage that is applied to the graphene, signified by V_{samp} . A voltage, V_{top} is also applied to the top gate that has been added to an oscillating signal from the function generator. The function generator also applies a signal to the reference capacitor. This is in line with a voltage that goes through a 100 M Ω resistor and then runs to the gate of a Fujitsu FHX35X low noise high electron mobility transistor (HEMT). The HEMT is used as an impedance matching amplifier. It is attached to a printed circuit board (PCB) vertically with solder. The mounting of the HEMT is vertical so that the two dimensional electron gas of the transistor is parallel to the magnetic field. This setup with the sample will create a balance point, labeled in Figure 4.1 (top left). This point balances the geometric capacitance of the device and any unimportant parasitic capacitance. The HEMT is voltage biased with a 1 k Ω resistor for stable operation around the maximal gain of the amplifier.

4.1.2 Cryostat to Measurement Electronics

The capacitance bridge, along with the DUT, is bonded to a sample holder (PPMS puck) that is lowered into a Quantum Design Evercool II cryostat. The PPMS is a cryostat that can achieve low temperatures, 2 Kelvin, and high magnetic field with a superconducting magnet, up to 9 Tesla. The device is wire bonded to a puck that is

inserted into the cryostat and connected with the internal electronics that we are able to access from outside of the cryostat through a breakout box that was made in the lab.

Outside of the cryostat, we have the electronic set up that includes a digital-to-analog/analog-to-digital converter (DAC-ADC), SR-830 lock-in amplifier, and a function generator. The DAC-ADC can supply a voltage ± 10 V and read a voltage on a chosen channel. The breakout box is used to make connections to the device inside of the cryostat.

4.2 Capacitance Measurements

With this set up, we measure the penetration field capacitance of the device. The penetration capacitance is related to the electronic compressibility. This gives a clear picture of the electronic states of the material. The penetration field capacitance can be written as[20]:

$$C_p = \frac{c^2}{2c + \frac{\partial n}{\partial \mu}} \quad (4.1)$$

where c is the geometric capacitance, μ is the chemical potential, and $\frac{\partial n}{\partial \mu}$ is the thermodynamic density of states[23] or bulk compressibility. At the balance point, we sweep V_{samp} and V_{top} to measure the changes in the penetration field capacitance for different charge density (n) and field polarization (p).

Chapter 5

Results

This chapter will go over the results that were obtained for this thesis. The capacitance was taken for each device by measuring the penetration capacitance (C_p). The penetration capacitance is normalized by the reference capacitor (C_{ref}) in the capacitance bridge. These values are measured by applying a small AC excitation to the top gate of the device and then adjusting the excitation on the reference capacitor to balance the bridge (see also figure 4.1). Once the balance point is found, we sweep the top and sample DC voltages to change the charge density (n_0) and the layer polarization (p_0). These are related through the following simple equations:

$$\frac{n_0}{c} = v_t + v_b \quad (5.1)$$

$$\frac{p_0}{c} = v_t - v_b \quad (5.2)$$

where v_t (v_b) is the top (bottom) gate voltage. The data we present will be the changes in the penetration field capacitance as a function of the charge density (number and type of charge carrier) and the layer polarization (the orientation and strength of the electric field that penetrates the stack). The penetration field capacitance will be relatively high (at the

balance point) when the graphene layer is insulating and low when the graphene layer is more conducting.

The chapter will start by reviewing the data that was taken on devices with monolayer graphene and MoS₂. Then, it will present the data from devices with bilayer graphene and MoS₂.

5.1 Monolayer Graphene on MoS₂

There are two monolayer devices that were tested. Both of these devices were fabricated with an MoS₂ flake below the graphene flake to investigate a spin orbit coupling proximity effect that has been reported in literature [44, 45, 46, 47]. It has been shown that when graphene is placed on top of a strong spin orbit coupling material, such as MoS₂, it will inherit some of this interaction through what is called a proximity effect. This proximity effect can lead to two types of induced spin orbit coupling, an ising spin orbit coupling and a Rashba spin orbit coupling. We aimed to investigate this proximity effect in our devices.

The first device presented is JMA002. Figure 5.1 shows an optical image of the device in panel **a**. This device was made with monolayer graphene that is in contact with the MoS₂. There is a piece of BN on each side of the graphene/MoS₂ to insulate it from the graphite gates that are on the outside of the stack. The schematic of the stacking order can be seen in figure 5.1(b).

Capacitance measurements for JMA002 were first taken without an applied magnetic field at 2 K in a cryostat. Figure 5.1(c) is the 2D plot of these measurements. The measurements resemble earlier reports of capacitance measurements of monolayer graphene [23]. C_p is plotted as a function of p_0/c on the vertical axis and n_0/c on the horizontal axis. The reduction in the density of states of graphene around the Dirac point can be seen at $n_0/c \approx 0$ as the peak in the capacitance signal. There is also a weak peak in the form of a

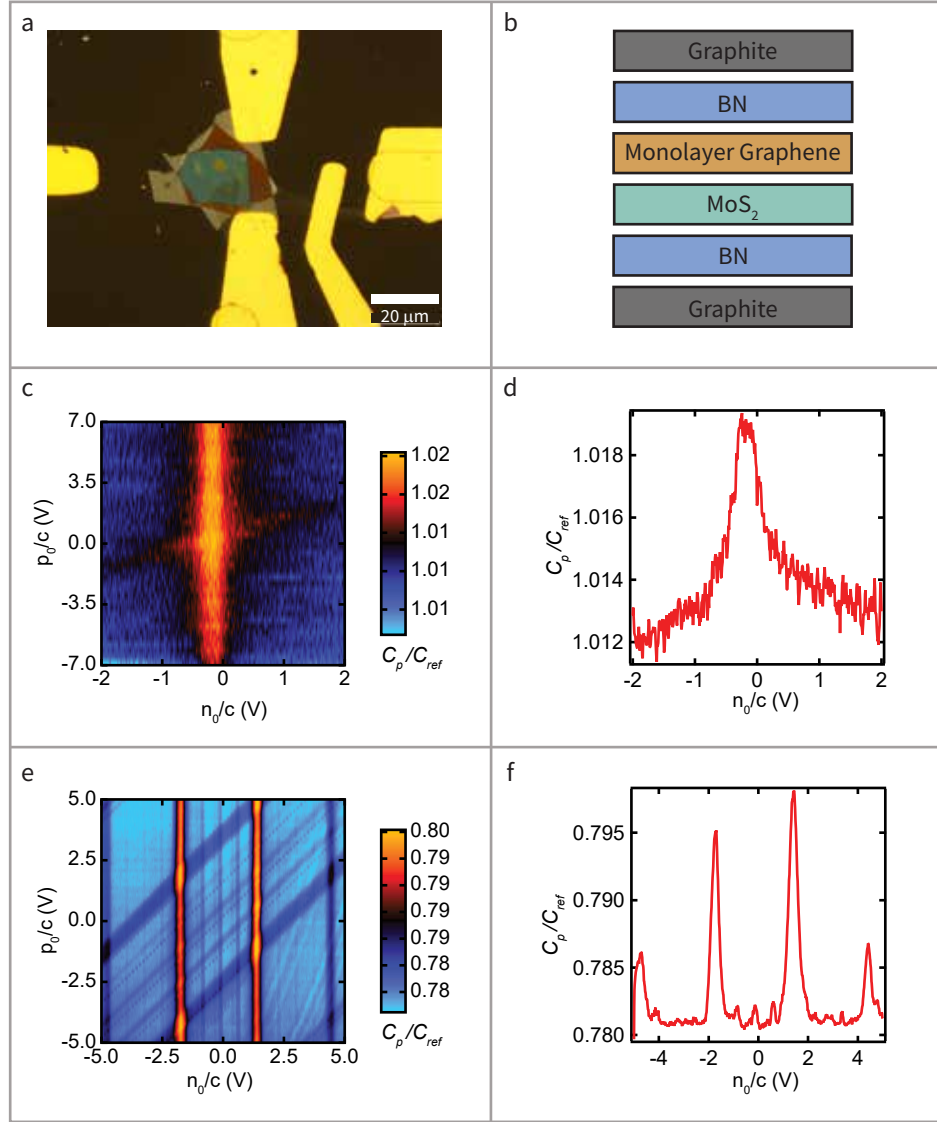


Figure 5.1: This figure shows data that was obtained from device JMA002. (a) An optical image of the device with patterned gold electrodes. (b) A digitally drawn schematic of the layers of JMA002. There is monolayer graphene in contact with MoS₂. These two materials are sandwiched on each side by BN and graphite gates. (c) 2D plot of the penetration capacitance (C_p), scaled by the reference capacitor (C_{ref}), plotted as a function of charge concentration (n_0/c) and polarization (p_0/c) taken at 2 K. (d) A line cut taken of plot in (c) at $p_0 = 7V$. The peak is due to the reduction in the DOS of the graphene flake. (e) 2D plot of C_p/C_{ref} as a function of n_0/c and p_0/c taken at 2 K and 9 T magnetic field. The plot shows the quantum hall gaps as vertical lines starting in the middle at 0 V and working outwards. (f) A line cut of plot of the data plotted in (e) taken at $p_0 = 5 V$. The filling factors can be seen as local maxima, starting at 0 V and working outwards.

diagonal line around $p_0/c = 0$ V. We do not know the precise origin of this weak peak, but it could come from another dislocated piece of graphene within the stack but with different gate coupling. Figure 5.1(d) shows a 1D plot where a line cut was taken at $p_0/c = 7$ V. The line has a peak at $n_0/c = 0$ V that comes from the graphene reduced DOS.

For the rest of the measurements that were taken, a magnetic field of 9 T was applied to the device. The 2D plot seen in figure 5.1(e) shows the integer quantum Hall gaps that arise[23]. They can be seen as peaks in the capacitance signal, with smaller peaks surrounding $n_0/c = 0$ V and with the largest peaks in capacitance at around $n_0/c = 2$ V, which corresponds to the 3 and -3 filling factors. Diagonal lines can be seen cutting through the signal that are picked up from the spurious graphene flake. A line cut of the 2D plot taken at $p_0/c = 5$ V is shown in figure 5.1(f) where the quantum Hall gaps are seen as the local maxima.

The second monolayer device is KC011. The optical image of the device can be seen in figure 5.2(a). The device has monolayer graphene with MoS₂ that has been sandwiched with BN and then graphite to use as the top and bottom gate (figure 5.2(b)).

The data that was taken for KC011 at 2 K with no external magnetic field can be seen in figure 5.2(c). This is a plot of the capacitance as a function of the charge concentration and the polarization. The bright orange line down the center of the 2D plot is due to the decrease in the DOS of graphene near the Dirac point. A diagonal dip (light blue) can also be seen in this plot. We are uncertain of the origin of this capacitance signal but it may be associated with spurious quantum capacitance changes in the thin gate electrodes. In figure 5.2(d), a line cut was taken of the 2D plot at a polarization of 4 V. The graphene Dirac point can be seen as the peak at $n_0/c = 0$ V.

Measurements were then taken with an applied magnetic field of 9 T. The results of these measurements can be seen in figure 5.4(e and f). The 2D plot shows the different integer quantum Hall gaps that occur due to the quantizing magnetic field. These can be seen as peaks in the capacitance values, starting at $n_0/c = 0$ V as the zeroth filling factor.

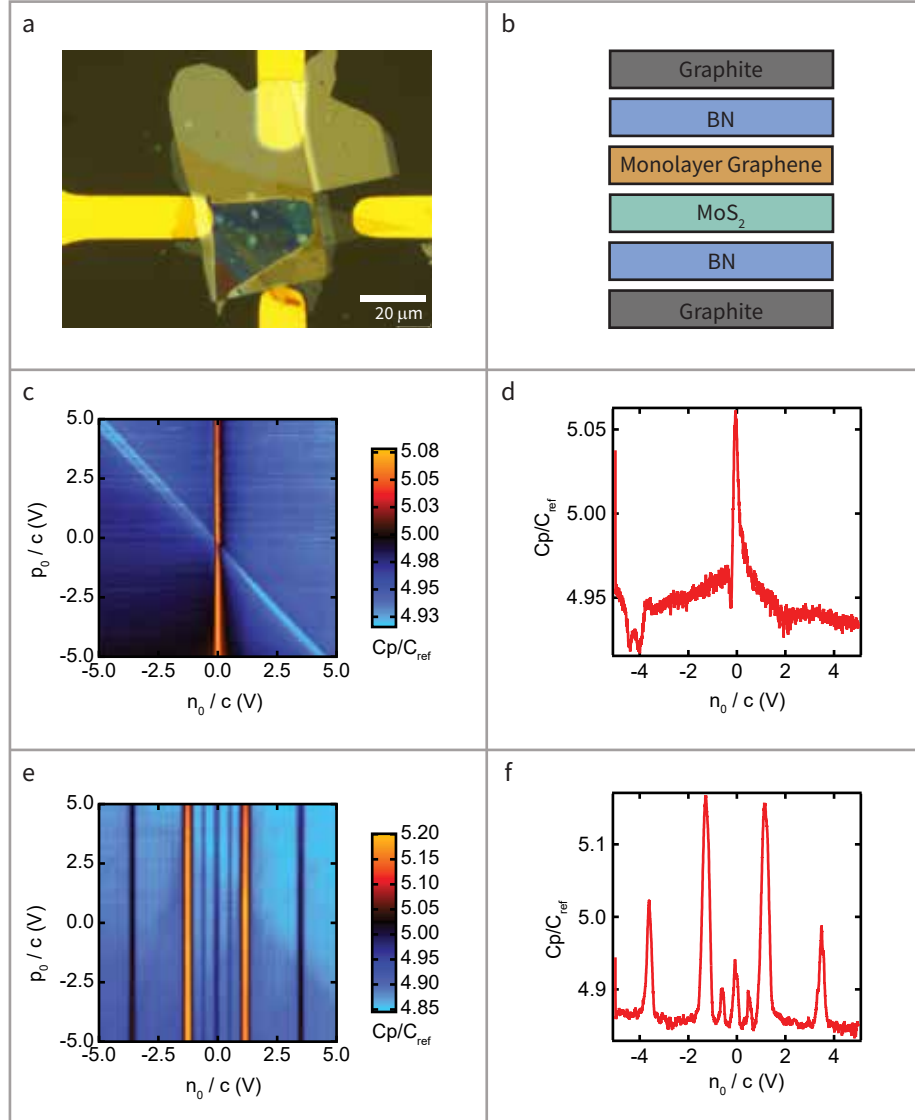


Figure 5.2: This figure shows the data that was obtained for device KC011. (a) An optical image of the device. (b) A digitally drawn schematic of the layers of KC011. There is monolayer graphene that is in contact with MoS₂. These two materials are sandwiched on each side by BN and graphite gates. (c) 2D plot of the penetration capacitance (C_p), scaled by the reference capacitor (C_{ref}), plotted as a function of charge concentration (n_0/c) and polarization (p_0/c) taken at 2 K. (d) A line cut of the data plotted in (c) at a polarization of 4 V. (e) 2D plot of the penetration capacitance (C_p), scaled by the reference capacitor (C_{ref}), plotted as a function of charge concentration (n_0/c) and polarization (p_0/c) taken at 2 K and 9 T. The quantum hall gaps show up in the plot as vertical lines, starting with 0 at $n_0/c = 0$ V and working outwards. (f) A line cut taken from plot (e) at $p_0/c = 5$ V. The quantum hall gaps can be seen as local maxima start in the middle at $n_0/c = 0$ V and working outwards.

The filling factors then work their way outwards from the center taking values 1, -1, 2, -2, etc. The 1D plot is a line cut taken at $p_0/c = 5$ V. The local maxima where the capacitance peaks are the various filling factors for the quantum hall gaps.

Summarizing our results on the monolayer graphene devices, we did not see a clear indication of the MoS₂ flake or its possible effect on the graphene capacitance signal. In order to further investigate these types of devices, we aim to perform weak antilocalization measurements which will allow us to extract charge scattering rates associated with spin orbit coupling [44].

5.2 Bilayer Graphene on MoS₂

Two bilayer devices were tested for this thesis. Both of these devices were fabricated with an MoS₂ flake incorporated in the stack.

Measurements for the device KC004 were first taken at room temperature. The optical image and the stacking schematic are shown in figures 5.3(a and b). In figure 5.3(c) the conduction band edge of the MoS₂ can be seen clearly. This edge delineates the insulating gap (red portion) from the conducting band (blue portion).

The device was then cooled down to 2 K, without an applied magnetic field (figure 5.4(a-b)). The 1D line cut of the plot was taken at $n_0/c = 5$ V, which shows a linear relationship between the capacitance and the polarization. This is because the transistor mount temperature was not stable, causing the amplifier to change over time producing a slowly varying capacitance signal. To remedy this, the background was subtracted by taking a line cut at $n_0/c = -5$ V and then subtracting it from each line of the 2D plot. This gives the plots from figure 5.4(c-d). The expected relationship is shown between the conduction band and band gap of the MoS₂, with the conduction band shown in blue and the band gap in red. There is a sharp peak in capacitance that can be seen as the orange line at $n_0/c = 0$ V. This peak is from the bilayer graphene. The 1D plot is a line cut taken

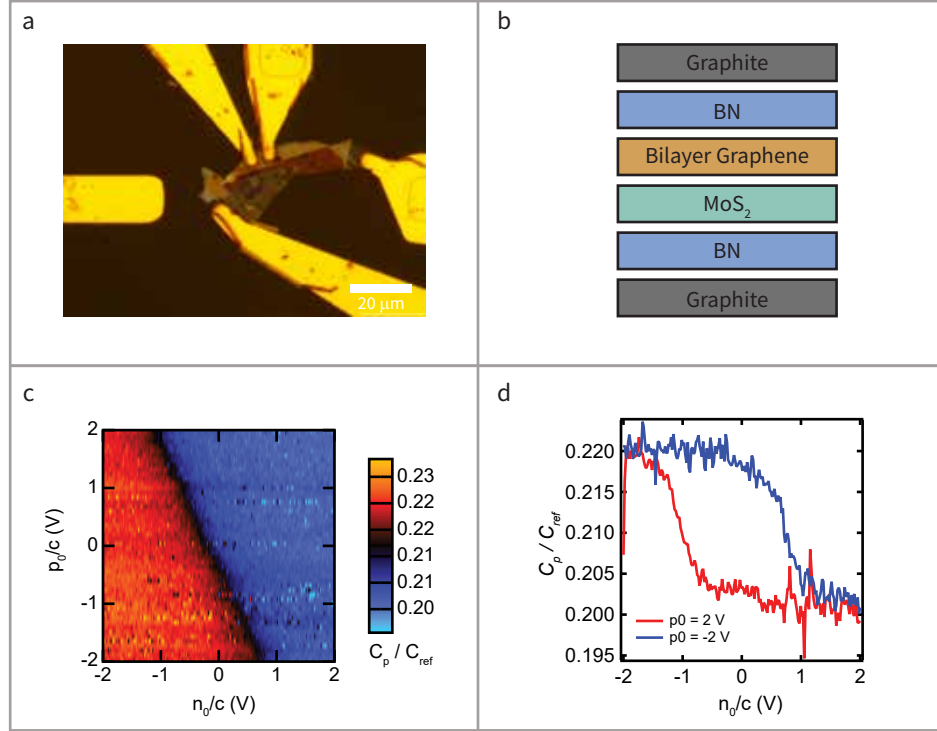


Figure 5.3: The room temperature (300 K) data taken for KC004 at no external magnetic field (0 T). (a) An optical image of the device. (b) A schematic of the layers of KC004. There is bilayer graphene flake in contact with MoS₂ that has been sandwiched on each side by a piece of BN and graphite. (c) A 2D plot with the penetration capacitance (C_p) scaled by the reference capacitance (C_{ref}) of the capacitance bridge as a function of the charge concentration (n_0/c) and the polarization (p_0/c). The difference between the red and the blue shows the conduction band edge of the MoS₂ where the right side of the graph is the conduction band. (d) A line cut taken of the data plotted in (c) taken at $p_0/c = 5$ V.

at $p_0/c = 5$ V. The graphene is the sharp peak, and the sharp decline at $n_0/c = 2$ V is the MoS₂ band edge.

We note that there is an asymmetry factor in our software that accounts for the difference in the top and bottom gate geometric capacitance. For plots in figure 5.3 and figure 5.4 the asymmetry factor was changed to reflect the charge density in the bilayer graphene at low temperature. This is the reason the orientation of the band edge for MoS₂ changes between these two data sets.

This data, although not ideal because of the varying capacitance signal of the amplifier, shows that we can resolve both the bilayer graphene and the MoS₂ flake in the same device.

The last device that was tested for this thesis is JMA003. The optical image of the device and the layer schematic is seen in figure 5.5(a-b). This device is made with bilayer graphene in contact with MoS₂.

The first set of data was taken at 2 K with no external magnetic field applied. The 2D plot (figure 5.5(c)) shows the band edge for MoS₂ at $n_0/c \approx 1.5$ V. The graphene band gap can be seen as the peak of capacitance at $n_0/c \approx -0.5$ V. A line cut of the plot in panel (d) was taken at $p_0/c = -3$ V. This plot clearly shows the graphene band gap as the maximum at $n_0/c \approx -0.5$ V, and the decline indicates the band edge of the MoS₂.

Figure 5.5(e-f) is the second set of data that was taken after the external magnetic field was applied to the device. The 2D plot shows the integer quantum Hall gaps of the bilayer graphene. These filling factors can be seen as vertical spikes in the capacitance. The filling factors can be seen even more clearly in the 1D plot, which was created by taking a line cut at $p_0/c = -5$ V, as the local maxima.

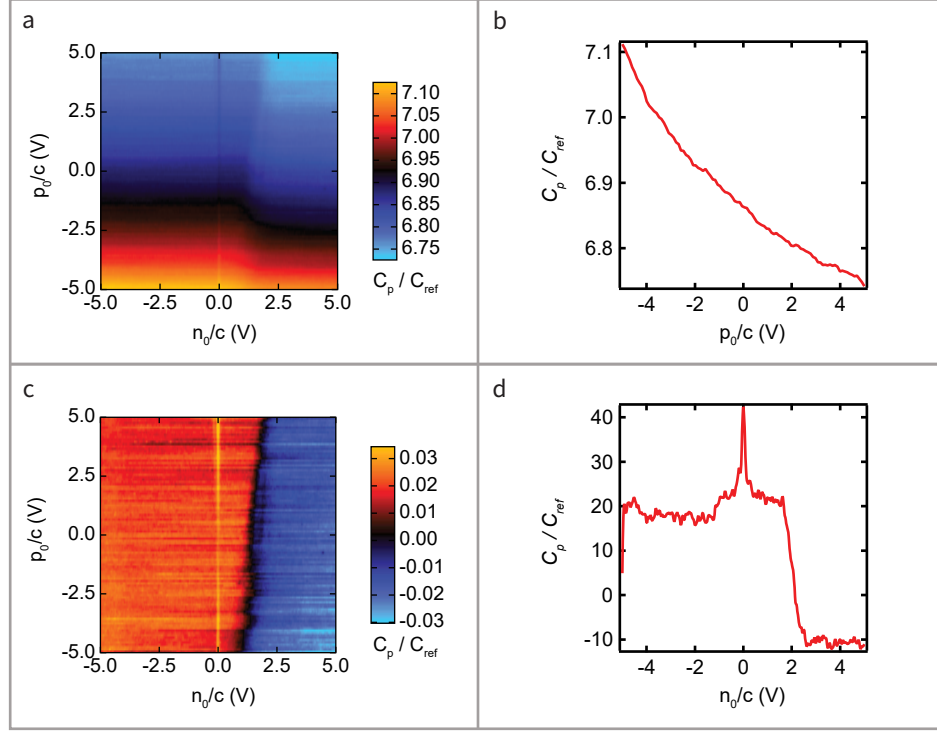


Figure 5.4: The data taken for KC004 at 2K with no external magnetic field. (a) The data for the scaled capacitance measurements as a function of charge concentration and polarization. The band edge of MoS_2 can be seen, but it is vertical. (b) A line cut taken of plot (a) taken at $n_0/c = 5$ V shows that the relationship is linear. (c) The background of plot (a) was subtracted by taking a line cut at $n_0/c = -5$ V and then subtracted from the rest of the lines of the plot. This gives us the expected vertical line of the MoS_2 and the band edge. The band gap of the bilayer graphene can also be seen as the slight yellow line. (d) A line cut was taken at $p_0/c = 5$ V of plot (c). At $n_0/c = 0$ V, there is a sharp peak from the band gap of the graphene. The red line then declines around $n_0/c = 2$ V indicating the MoS_2 band edge.

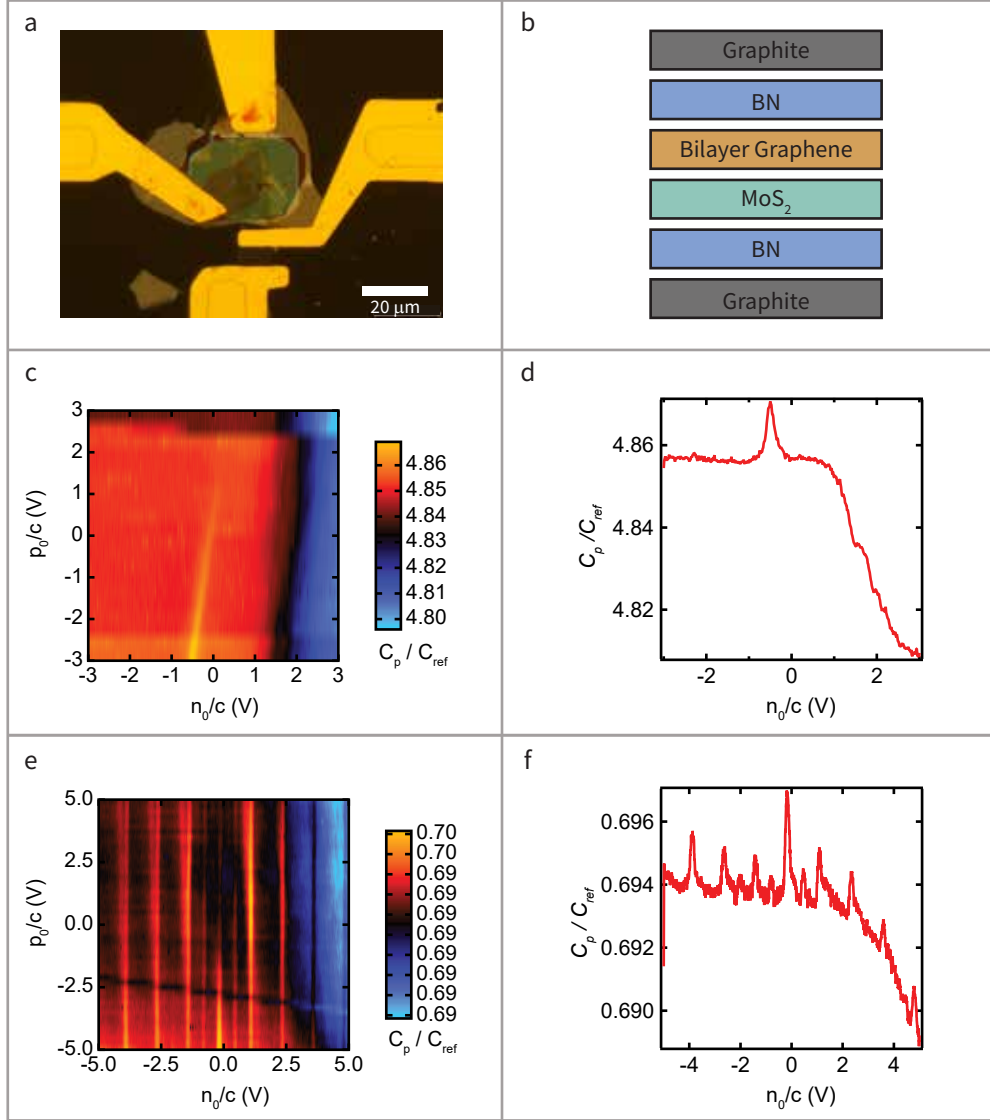


Figure 5.5: The data taken for the device JMA003. (a) An optical image of the device with the patterned electrodes. (b) A layer schematic of the device. This device has bilayer graphene in contact with MoS₂ that is sandwiched between BN and graphite on both sides. (c) A 2D plot taken at 2 K with no applied magnetic field (0 T). It shows the penetration capacitance scaled by the reference capacitance of the capacitance bridge (C_p/C_{ref}) as a function of the charge concentration (n_0/c) and the polarization (p_0/c). The band edge of the MoS₂ can be seen on the right of the graph, represented by the change in colors from red to blue. (d) A line cut of plot (c) taken at $p_0/c = -3$ V. This shows the band gap of the graphene around $n_0/c = -0.5$ V as the sharp peak. The band edge of the MoS₂ is seen around $n_0/c = 1.5$ V indicated by the decline. (e) C_p/C_{ref} as a function of n_0/c and p_0/c taken for the device at a temperature of 2 K and with an applied magnetic field of 9 T. This plot shows the quantum Hall gaps of the bilayer graphene. (f) A line cut taken of plot (e) at $p_0/c = -5$ V. The local maxima are the quantum Hall gaps of the bilayer graphene.

Chapter 6

Discussion and Future Work

We have shown that we are able to make highly sensitive capacitance measurements of van der Waals heterostructures using several devices. Measurements were taken in monolayer and bilayer graphene devices. Both of the graphene stacks included contact with MoS₂. The measurements of these devices were taken at different temperatures with or without an applied magnetic field. The devices that have the external magnetic field show clear integer quantum Hall gaps. In the measurements taken without an applied magnetic field, the band gap of graphene can be seen and the band edge of MoS₂ can be confirmed in a few devices.

There are multiple ways in which we can improve on further fabrication and measurement processes. The masking and etching process doesn't produce as clean of results as we would like. With updates to this process, we can create devices with less overlap and more certainty that we are making connections with the pieces of the device that we are wanting. Another thing that needs some perfecting is the capacitance bridge. Some of the measurements were dominated by noise. Rethinking what parts we use and redesigning how we build the capacitance bridge will help us get even better measurement results.

After these improvements are made, we will look at other ways to attempt to observe

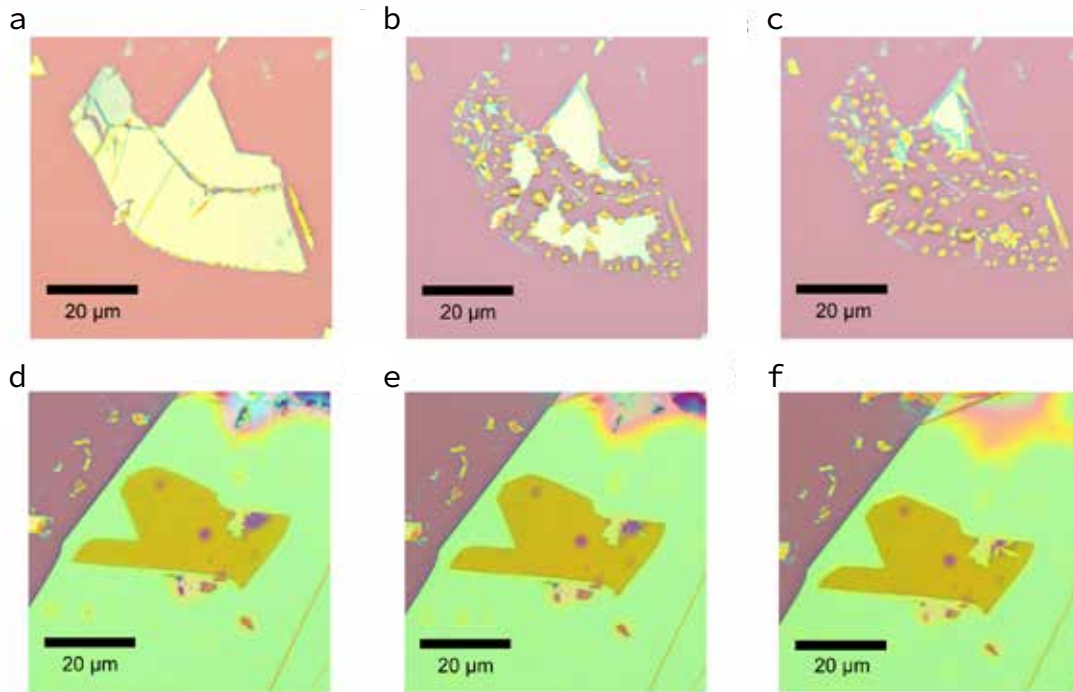


Figure 6.1: The degradation in ambient conditions and passivation of Chromium triiodide(CrI_3). Panel (a-c) are optical images of CrI_3 in ambient conditions taken at (a) 10 minutes, (b) 15 minutes, and (c) 50 minutes. Panel (d-f) are optical images of CrI_3 after being layered by BN taken at (d) 10 minutes, (e) 15 minutes, and (f) 50 minutes in ambient conditions.

these systems. One of these ways is by incorporating a magnetic material. The devices that were used for this these were all made with MoS_2 for its strong spin orbit coupling energy, but we would like to see if we would get the same results by using a material that has intrinsic magnetism. Previously, we have done work with chromium tri-iodide (CrI_3), a layered ferromagnetic semiconductor [48, 49]. One of the hardships of using CrI_3 is its degradation time in ambient conditions [50, 51]. Figure 6.1(a-c) shows optical images of how quickly it degrades. After 50 minutes, the flake of CrI_3 is almost completely dissolved. We were able to successfully passivate CrI_3 by covering the area of the flake with BN (figure 6.1(d-f)). Knowing this, we believe that we will be able to fully encapsulate the CrI_3 in a stack and prevent it from degrading. We can then repeat the capacitance measurements with CrI_3 in place of MoS_2 .

It has been theorized that stacking graphene in between a material with a strong spin orbit coupling and a material that is intrinsically magnetic will result in a definite QAHE [1]. To achieve these results, we would like to fabricate a device that has bilayer graphene in between a layer of MoS_2 and CrI_3 . With the way the device is fabricated, we hope to fully encapsulate the CrI_3 . We would then perform capacitance measurements, in hopes to realize the QAHE.

Appendix

Attached are the permissions received for the figures used in this thesis.



13-Apr-2022

This license agreement between the American Physical Society ("APS") and Kayla Cerminara ("You") consists of your license details and the terms and conditions provided by the American Physical Society and SciPris.

Licensed Content Information

License Number:	RNP/22/APR/052578
License date:	13-Apr-2022
DOI:	10.1103/PhysRevB.104.L161113
Title:	Valley-polarized quantum anomalous Hall phase in bilayer graphene with layer-dependent proximity effects
Author:	Marc Vila, Jose H. Garcia, and Stephan Roche
Publication:	Physical Review B
Publisher:	American Physical Society
Cost:	USD \$ 0.00

Request Details

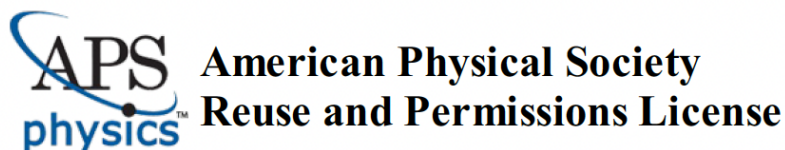
Does your reuse require significant modifications:	No
Specify intended distribution locations:	United States
Reuse Category:	Reuse in a thesis/dissertation
Requestor Type:	Student
Items for Reuse:	Figures/Tables
Number of Figure/Tables:	2
Figure/Tables Details:	Figure 1 and Figure 4a
Format for Reuse:	Electronic and Print
Total number of print copies:	Up to 1000

Information about New Publication:

University/Publisher:	University of Nevada, Las Vegas
Title of dissertation/thesis:	Towards highly sensitive capacitance measurements of a quantum anomalous Hall phase in van der Waals heterostructures
Author(s):	Kayla Cerminara
Expected completion date:	May, 2022

License Requestor Information

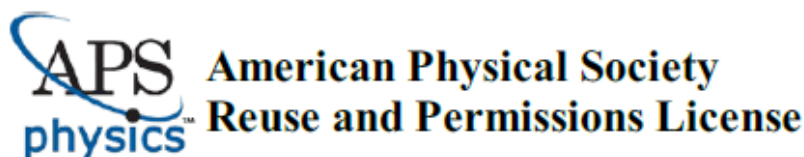
Name:	Kayla Cerminara
Affiliation:	Individual
Email Id:	kcermina@unlv.nevada.edu
Country:	United States



TERMS AND CONDITIONS

The American Physical Society (APS) is pleased to grant the Requestor of this license a non-exclusive, non-transferable permission, limited to Electronic and Print format, provided all criteria outlined below are followed.

1. You must also obtain permission from at least one of the lead authors for each separate work, if you haven't done so already. The author's name and affiliation can be found on the first page of the published Article.
2. For electronic format permissions, Requestor agrees to provide a hyperlink from the reprinted APS material using the source material's DOI on the web page where the work appears. The hyperlink should use the standard DOI resolution URL, <http://dx.doi.org/{DOI}>. The hyperlink may be embedded in the copyright credit line.
3. For print format permissions, Requestor agrees to print the required copyright credit line on the first page where the material appears: "Reprinted (abstract/excerpt/figure) with permission from [(FULL REFERENCE CITATION) as follows: Author's Names, APS Journal Title, Volume Number, Page Number and Year of Publication.] Copyright (YEAR) by the American Physical Society."
4. Permission granted in this license is for a one-time use and does not include permission for any future editions, updates, databases, formats or other matters. Permission must be sought for any additional use.
5. Use of the material does not and must not imply any endorsement by APS.
6. APS does not imply, purport or intend to grant permission to reuse materials to which it does not hold copyright. It is the requestor's sole responsibility to ensure the licensed material is original to APS and does not contain the copyright of another entity, and that the copyright notice of the figure, photograph, cover or table does not indicate it was reprinted by APS with permission from another source.
7. The permission granted herein is personal to the Requestor for the use specified and is not transferable or assignable without express written permission of APS. This license may not be amended except in writing by APS.
8. You may not alter, edit or modify the material in any manner.
9. You may translate the materials only when translation rights have been granted.
10. APS is not responsible for any errors or omissions due to translation.
11. You may not use the material for promotional, sales, advertising or marketing purposes.
12. The foregoing license shall not take effect unless and until APS or its agent, Aptara, receives payment in full in accordance with Aptara Billing and Payment Terms and Conditions, which are incorporated herein by reference.
13. Should the terms of this license be violated at any time, APS or Aptara may revoke the license with no refund to you and seek relief to the fullest extent of the laws of the USA. Official written notice will be made using the contact information provided with the permission request. Failure to receive such notice will not nullify revocation of the permission.
14. APS reserves all rights not specifically granted herein.
15. This document, including the Aptara Billing and Payment Terms and Conditions, shall be the entire agreement between the parties relating to the subject matter hereof.



12-Apr-2022

This license agreement between the American Physical Society ("APS") and Kayla Cerminara ("You") consists of your license details and the terms and conditions provided by the American Physical Society and SciPris.

Licensed Content Information

License Number:	RNP/22/APR/052533
License date:	12-Apr-2022
DOI:	10.1103/RevModPhys.81.109
Title:	The electronic properties of graphene
Author:	A. H. Castro Neto et al.
Publication:	Reviews of Modern Physics
Publisher:	American Physical Society
Cost:	USD \$ 0.00

Request Details

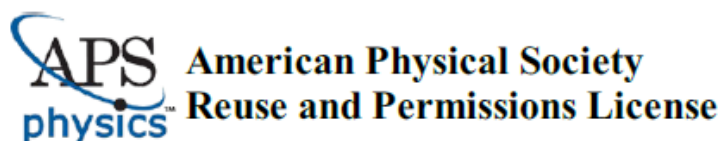
Does your reuse require significant modifications:	No
Specify intended distribution locations:	United States
Reuse Category:	Reuse in a thesis/dissertation
Requestor Type:	Student
Items for Reuse:	Figures/Tables
Number of Figure/Tables:	2
Figure/Tables Details:	Figure 1 and Figure 2
Format for Reuse:	Print and Electronic
Total number of print copies:	Up to 1000

Information about New Publication:

University/Publisher:	University of Nevada, Las Vegas
Title of dissertation/thesis:	Towards highly sensitive capacitance measurements of a quantum anomalous Hall phase in van der Waals heterostructures
Author(s):	Kayla Cerminara
Expected completion date:	May, 2022

License Requestor Information

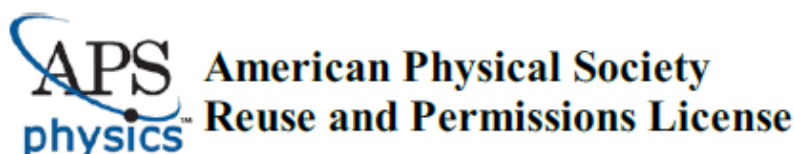
Name:	Kayla Cerminara
Affiliation:	Individual
Email Id:	kcermina@unlv.nevada.edu



TERMS AND CONDITIONS

The American Physical Society (APS) is pleased to grant the Requestor of this license a non-exclusive, non-transferable permission, limited to Print and Electronic format, provided all criteria outlined below are followed.

1. You must also obtain permission from at least one of the lead authors for each separate work, if you haven't done so already. The author's name and affiliation can be found on the first page of the published Article.
2. For electronic format permissions, Requestor agrees to provide a hyperlink from the reprinted APS material using the source material's DOI on the web page where the work appears. The hyperlink should use the standard DOI resolution URL, <http://dx.doi.org/{DOI}>. The hyperlink may be embedded in the copyright credit line.
3. For print format permissions, Requestor agrees to print the required copyright credit line on the first page where the material appears: "Reprinted (abstract/excerpt/figure) with permission from [(FULL REFERENCE CITATION) as follows: Author's Names, APS Journal Title, Volume Number, Page Number and Year of Publication.] Copyright (YEAR) by the American Physical Society."
4. Permission granted in this license is for a one-time use and does not include permission for any future editions, updates, databases, formats or other matters. Permission must be sought for any additional use.
5. Use of the material does not and must not imply any endorsement by APS.
6. APS does not imply, purport or intend to grant permission to reuse materials to which it does not hold copyright. It is the requestor's sole responsibility to ensure the licensed material is original to APS and does not contain the copyright of another entity, and that the copyright notice of the figure, photograph, cover or table does not indicate it was reprinted by APS with permission from another source.
7. The permission granted herein is personal to the Requestor for the use specified and is not transferable or assignable without express written permission of APS. This license may not be amended except in writing by APS.
8. You may not alter, edit or modify the material in any manner.
9. You may translate the materials only when translation rights have been granted.
10. APS is not responsible for any errors or omissions due to translation.
11. You may not use the material for promotional, sales, advertising or marketing purposes.
12. The foregoing license shall not take effect unless and until APS or its agent, Aptara, receives payment in full in accordance with Aptara Billing and Payment Terms and Conditions, which are incorporated herein by reference.
13. Should the terms of this license be violated at any time, APS or Aptara may revoke the license with no refund to you and seek relief to the fullest extent of the laws of the USA. Official written notice will be made using the contact information provided with the permission request. Failure to receive such notice will not nullify revocation of the permission.
14. APS reserves all rights not specifically granted herein.
15. This document, including the Aptara Billing and Payment Terms and Conditions, shall be the entire agreement between the parties relating to the subject matter hereof.



12-Apr-2022

This license agreement between the American Physical Society ("APS") and Kayla Cerminara ("You") consists of your license details and the terms and conditions provided by the American Physical Society and SciPris.

Licensed Content Information

License Number:	RNP/22/APR/052534
License date:	12-Apr-2022
DOI:	10.1103/PhysRevB.88.085433
Title:	Three-band tight-binding model for monolayers of group-VIB transition metal dichalcogenides
Author:	Gui-Bin Liu et al.
Publication:	Physical Review B
Publisher:	American Physical Society
Cost:	USD \$ 0.00

Request Details

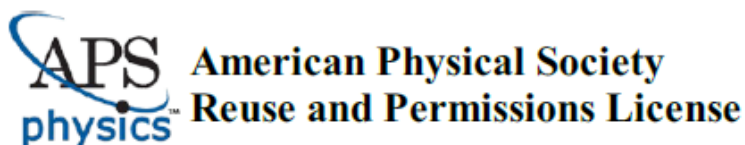
Does your reuse require significant modifications:	No
Specify intended distribution locations:	United States
Reuse Category:	Reuse in a thesis/dissertation
Requestor Type:	Student
Items for Reuse:	Figures/Tables
Number of Figure/Tables:	1
Figure/Tables Details:	Figure 2
Format for Reuse:	Print and Electronic
Total number of print copies:	Up to 1000

Information about New Publication:

University/Publisher:	University of Nevada, Las Vegas
Title of dissertation/thesis:	Towards highly sensitive capacitance measurements of a quantum anomalous Hall phase in van der Waals heterostructures
Author(s):	Kayla Cerminara
Expected completion date:	May, 2022

License Requestor Information

Name:	Kayla Cerminara
Affiliation:	Individual
Email Id:	kcermina@unlv.nevada.edu
Country:	United States



TERMS AND CONDITIONS

The American Physical Society (APS) is pleased to grant the Requestor of this license a non-exclusive, non-transferable permission, limited to Print and Electronic format, provided all criteria outlined below are followed.

1. You must also obtain permission from at least one of the lead authors for each separate work, if you haven't done so already. The author's name and affiliation can be found on the first page of the published Article.
2. For electronic format permissions, Requestor agrees to provide a hyperlink from the reprinted APS material using the source material's DOI on the web page where the work appears. The hyperlink should use the standard DOI resolution URL, <http://dx.doi.org/{DOI}>. The hyperlink may be embedded in the copyright credit line.
3. For print format permissions, Requestor agrees to print the required copyright credit line on the first page where the material appears: "Reprinted (abstract/excerpt/figure) with permission from [(FULL REFERENCE CITATION) as follows: Author's Names, APS Journal Title, Volume Number, Page Number and Year of Publication.] Copyright (YEAR) by the American Physical Society."
4. Permission granted in this license is for a one-time use and does not include permission for any future editions, updates, databases, formats or other matters. Permission must be sought for any additional use.
5. Use of the material does not and must not imply any endorsement by APS.
6. APS does not imply, purport or intend to grant permission to reuse materials to which it does not hold copyright. It is the requestor's sole responsibility to ensure the licensed material is original to APS and does not contain the copyright of another entity, and that the copyright notice of the figure, photograph, cover or table does not indicate it was reprinted by APS with permission from another source.
7. The permission granted herein is personal to the Requestor for the use specified and is not transferable or assignable without express written permission of APS. This license may not be amended except in writing by APS.
8. You may not alter, edit or modify the material in any manner.
9. You may translate the materials only when translation rights have been granted.
10. APS is not responsible for any errors or omissions due to translation.
11. You may not use the material for promotional, sales, advertising or marketing purposes.
12. The foregoing license shall not take effect unless and until APS or its agent, Aptara, receives payment in full in accordance with Aptara Billing and Payment Terms and Conditions, which are incorporated herein by reference.
13. Should the terms of this license be violated at any time, APS or Aptara may revoke the license with no refund to you and seek relief to the fullest extent of the laws of the USA. Official written notice will be made using the contact information provided with the permission request. Failure to receive such notice will not nullify revocation of the permission.
14. APS reserves all rights not specifically granted herein.
15. This document, including the Aptara Billing and Payment Terms and Conditions, shall be the entire agreement between the parties relating to the subject matter hereof.

ELSEVIER LICENSE
TERMS AND CONDITIONS

Apr 18, 2022

This Agreement between University of Nevada, Las Vegas -- Kayla Cerminara ("You") and Elsevier ("Elsevier") consists of your license details and the terms and conditions provided by Elsevier and Copyright Clearance Center.

License Number	5286740499596
License date	Apr 12, 2022
Licensed Content Publisher	Elsevier
Licensed Content Publication	Elsevier Books
Licensed Content Title	Semiconductors and Semimetals
Licensed Content Author	G.R. Bhimanapati,N.R. Glavin,J.A. Robinson
Licensed Content Date	Jan 1, 2016
Licensed Content Pages	47
Start Page	101
End Page	147
Type of Use	reuse in a thesis/dissertation
Portion	figures/tables/illustrations

Number of figures/tables/illustrations	1
Format	both print and electronic
Are you the author of this Elsevier chapter?	No
Will you be translating?	No
Title	Towards highly sensitive capacitance measurements of a quantum anomalous Hall phase in van der Waals heterostructures
Institution name	University of Nevada, Las Vegas
Expected presentation date	May 2022
Portions	Figure 1a and Figure 1b
Requestor Location	University of Nevada, Las Vegas 9705 Treeline Run Ave. LAS VEGAS, NV 89166 United States Attn: University of Nevada, Las Vegas
Publisher Tax ID	98-0397604
Total	0.00 USD
Terms and Conditions	

INTRODUCTION

1. The publisher for this copyrighted material is Elsevier. By clicking "accept" in connection with completing this licensing transaction, you agree that the following terms and conditions apply to this transaction (along with the Billing and Payment terms and conditions established by Copyright Clearance Center, Inc. ("CCC"), at the time that you opened your Rightslink account and that are available at any time at <http://myaccount.copyright.com>).

GENERAL TERMS

2. Elsevier hereby grants you permission to reproduce the aforementioned material subject to the terms and conditions indicated.

3. Acknowledgement: If any part of the material to be used (for example, figures) has appeared in our publication with credit or acknowledgement to another source, permission must also be sought from that source. If such permission is not obtained then that material may not be included in your publication/copies. Suitable acknowledgement to the source must be made, either as a footnote or in a reference list at the end of your publication, as follows:

"Reprinted from Publication title, Vol /edition number, Author(s), Title of article / title of chapter, Pages No., Copyright (Year), with permission from Elsevier [OR APPLICABLE SOCIETY COPYRIGHT OWNER]." Also Lancet special credit - "Reprinted from The Lancet, Vol. number, Author(s), Title of article, Pages No., Copyright (Year), with permission from Elsevier."

4. Reproduction of this material is confined to the purpose and/or media for which permission is hereby given.

5. Altering/Modifying Material: Not Permitted. However figures and illustrations may be altered/adapted minimally to serve your work. Any other abbreviations, additions, deletions and/or any other alterations shall be made only with prior written authorization of Elsevier Ltd. (Please contact Elsevier's permissions helpdesk [here](#)). No modifications can be made to any Lancet figures/tables and they must be reproduced in full.

6. If the permission fee for the requested use of our material is waived in this instance, please be advised that your future requests for Elsevier materials may attract a fee.

7. Reservation of Rights: Publisher reserves all rights not specifically granted in the combination of (i) the license details provided by you and accepted in the course of this licensing transaction, (ii) these terms and conditions and (iii) CCC's Billing and Payment terms and conditions.

8. License Contingent Upon Payment: While you may exercise the rights licensed immediately upon issuance of the license at the end of the licensing process for the transaction, provided that you have disclosed complete and accurate details of your proposed use, no license is finally effective unless and until full payment is received from you (either by publisher or by CCC) as provided in CCC's Billing and Payment terms and conditions. If full payment is not received on a timely basis, then any license preliminarily granted shall be deemed automatically revoked and shall be void as if never granted. Further, in the event that you breach any of these terms and conditions or any of CCC's Billing and Payment terms and conditions, the license is automatically revoked and shall be void as if never granted. Use of materials as described in a revoked license, as well as any use of the materials beyond the scope of an unrevoked license, may constitute copyright infringement and publisher reserves the right to take any and all action to protect its copyright in the materials.

9. Warranties: Publisher makes no representations or warranties with respect to the licensed material.

10. Indemnity: You hereby indemnify and agree to hold harmless publisher and CCC, and their respective officers, directors, employees and agents, from and against any and all

claims arising out of your use of the licensed material other than as specifically authorized pursuant to this license.

11. **No Transfer of License:** This license is personal to you and may not be sublicensed, assigned, or transferred by you to any other person without publisher's written permission.

12. **No Amendment Except in Writing:** This license may not be amended except in a writing signed by both parties (or, in the case of publisher, by CCC on publisher's behalf).

13. **Objection to Contrary Terms:** Publisher hereby objects to any terms contained in any purchase order, acknowledgment, check endorsement or other writing prepared by you, which terms are inconsistent with these terms and conditions or CCC's Billing and Payment terms and conditions. These terms and conditions, together with CCC's Billing and Payment terms and conditions (which are incorporated herein), comprise the entire agreement between you and publisher (and CCC) concerning this licensing transaction. In the event of any conflict between your obligations established by these terms and conditions and those established by CCC's Billing and Payment terms and conditions, these terms and conditions shall control.

14. **Revocation:** Elsevier or Copyright Clearance Center may deny the permissions described in this License at their sole discretion, for any reason or no reason, with a full refund payable to you. Notice of such denial will be made using the contact information provided by you. Failure to receive such notice will not alter or invalidate the denial. In no event will Elsevier or Copyright Clearance Center be responsible or liable for any costs, expenses or damage incurred by you as a result of a denial of your permission request, other than a refund of the amount(s) paid by you to Elsevier and/or Copyright Clearance Center for denied permissions.

LIMITED LICENSE

The following terms and conditions apply only to specific license types:

15. **Translation:** This permission is granted for non-exclusive world **English** rights only unless your license was granted for translation rights. If you licensed translation rights you may only translate this content into the languages you requested. A professional translator must perform all translations and reproduce the content word for word preserving the integrity of the article.

16. **Posting licensed content on any Website:** The following terms and conditions apply as follows: Licensing material from an Elsevier journal: All content posted to the web site must maintain the copyright information line on the bottom of each image; A hyper-text must be included to the Homepage of the journal from which you are licensing at <http://www.sciencedirect.com/science/journal/xxxxx> or the Elsevier homepage for books at <http://www.elsevier.com>; Central Storage: This license does not include permission for a scanned version of the material to be stored in a central repository such as that provided by Heron/XanEdu.

Licensing material from an Elsevier book: A hyper-text link must be included to the Elsevier homepage at <http://www.elsevier.com>. All content posted to the web site must maintain the copyright information line on the bottom of each image.

Posting licensed content on Electronic reserve: In addition to the above the following clauses are applicable: The web site must be password-protected and made available only to

bona fide students registered on a relevant course. This permission is granted for 1 year only. You may obtain a new license for future website posting.

17. For journal authors: the following clauses are applicable in addition to the above:

Preprints:

A preprint is an author's own write-up of research results and analysis, it has not been peer-reviewed, nor has it had any other value added to it by a publisher (such as formatting, copyright, technical enhancement etc.).

Authors can share their preprints anywhere at any time. Preprints should not be added to or enhanced in any way in order to appear more like, or to substitute for, the final versions of articles however authors can update their preprints on arXiv or RePEc with their Accepted Author Manuscript (see below).

If accepted for publication, we encourage authors to link from the preprint to their formal publication via its DOI. Millions of researchers have access to the formal publications on ScienceDirect, and so links will help users to find, access, cite and use the best available version. Please note that Cell Press, The Lancet and some society-owned have different preprint policies. Information on these policies is available on the journal homepage.

Accepted Author Manuscripts: An accepted author manuscript is the manuscript of an article that has been accepted for publication and which typically includes author-incorporated changes suggested during submission, peer review and editor-author communications.

Authors can share their accepted author manuscript:

- immediately
 - via their non-commercial person homepage or blog
 - by updating a preprint in arXiv or RePEc with the accepted manuscript
 - via their research institute or institutional repository for internal institutional uses or as part of an invitation-only research collaboration work-group
 - directly by providing copies to their students or to research collaborators for their personal use
 - for private scholarly sharing as part of an invitation-only work group on commercial sites with which Elsevier has an agreement
- After the embargo period
 - via non-commercial hosting platforms such as their institutional repository
 - via commercial sites with which Elsevier has an agreement

In all cases accepted manuscripts should:

- link to the formal publication via its DOI
- bear a CC-BY-NC-ND license - this is easy to do
- if aggregated with other manuscripts, for example in a repository or other site, be shared in alignment with our hosting policy not be added to or enhanced in any way to appear more like, or to substitute for, the published journal article.

Published journal article (JPA): A published journal article (PJA) is the definitive final record of published research that appears or will appear in the journal and embodies all value-adding publishing activities including peer review co-ordination, copy-editing, formatting, (if relevant) pagination and online enrichment.

Policies for sharing publishing journal articles differ for subscription and gold open access articles:

Subscription Articles: If you are an author, please share a link to your article rather than the full-text. Millions of researchers have access to the formal publications on ScienceDirect, and so links will help your users to find, access, cite, and use the best available version.

Theses and dissertations which contain embedded PJAs as part of the formal submission can be posted publicly by the awarding institution with DOI links back to the formal publications on ScienceDirect.

If you are affiliated with a library that subscribes to ScienceDirect you have additional private sharing rights for others' research accessed under that agreement. This includes use for classroom teaching and internal training at the institution (including use in course packs and courseware programs), and inclusion of the article for grant funding purposes.

Gold Open Access Articles: May be shared according to the author-selected end-user license and should contain a [CrossMark logo](#), the end user license, and a DOI link to the formal publication on ScienceDirect.

Please refer to Elsevier's [posting policy](#) for further information.

18. For book authors the following clauses are applicable in addition to the above: Authors are permitted to place a brief summary of their work online only. You are not allowed to download and post the published electronic version of your chapter, nor may you scan the printed edition to create an electronic version. **Posting to a repository:** Authors are permitted to post a summary of their chapter only in their institution's repository.

19. Thesis/Dissertation: If your license is for use in a thesis/dissertation your thesis may be submitted to your institution in either print or electronic form. Should your thesis be published commercially, please reapply for permission. These requirements include permission for the Library and Archives of Canada to supply single copies, on demand, of the complete thesis and include permission for Proquest/UMI to supply single copies, on demand, of the complete thesis. Should your thesis be published commercially, please reapply for permission. Theses and dissertations which contain embedded PJAs as part of the formal submission can be posted publicly by the awarding institution with DOI links back to the formal publications on ScienceDirect.

Elsevier Open Access Terms and Conditions

You can publish open access with Elsevier in hundreds of open access journals or in nearly 2000 established subscription journals that support open access publishing. Permitted third party re-use of these open access articles is defined by the author's choice of Creative Commons user license. See our [open access license policy](#) for more information.

Terms & Conditions applicable to all Open Access articles published with Elsevier:

Any reuse of the article must not represent the author as endorsing the adaptation of the article nor should the article be modified in such a way as to damage the author's honour or reputation. If any changes have been made, such changes must be clearly indicated.

The author(s) must be appropriately credited and we ask that you include the end user license and a DOI link to the formal publication on ScienceDirect.

If any part of the material to be used (for example, figures) has appeared in our publication with credit or acknowledgement to another source it is the responsibility of the user to ensure their reuse complies with the terms and conditions determined by the rights holder.

Additional Terms & Conditions applicable to each Creative Commons user license:

CC BY: The CC-BY license allows users to copy, to create extracts, abstracts and new works from the Article, to alter and revise the Article and to make commercial use of the Article (including reuse and/or resale of the Article by commercial entities), provided the user gives appropriate credit (with a link to the formal publication through the relevant DOI), provides a link to the license, indicates if changes were made and the licensor is not represented as endorsing the use made of the work. The full details of the license are available at <http://creativecommons.org/licenses/by/4.0>.

CC BY NC SA: The CC BY-NC-SA license allows users to copy, to create extracts, abstracts and new works from the Article, to alter and revise the Article, provided this is not done for commercial purposes, and that the user gives appropriate credit (with a link to the formal publication through the relevant DOI), provides a link to the license, indicates if changes were made and the licensor is not represented as endorsing the use made of the work. Further, any new works must be made available on the same conditions. The full details of the license are available at <http://creativecommons.org/licenses/by-nc-sa/4.0>.

CC BY NC ND: The CC BY-NC-ND license allows users to copy and distribute the Article, provided this is not done for commercial purposes and further does not permit distribution of the Article if it is changed or edited in any way, and provided the user gives appropriate credit (with a link to the formal publication through the relevant DOI), provides a link to the license, and that the licensor is not represented as endorsing the use made of the work. The full details of the license are available at <http://creativecommons.org/licenses/by-nc-nd/4.0>. Any commercial reuse of Open Access articles published with a CC BY NC SA or CC BY NC ND license requires permission from Elsevier and will be subject to a fee.

Commercial reuse includes:

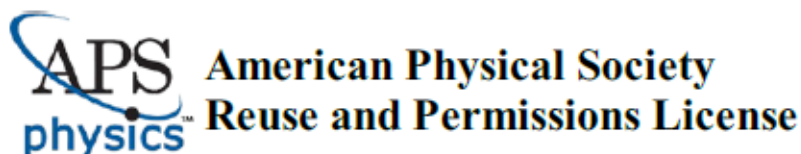
- Associating advertising with the full text of the Article
- Charging fees for document delivery or access
- Article aggregation
- Systematic distribution via e-mail lists or share buttons

Posting or linking by commercial companies for use by customers of those companies.

20. Other Conditions:

v1.10

Questions? customercare@copyright.com or +1-855-239-3415 (toll free in the US) or +1-978-646-2777.



12-Apr-2022

This license agreement between the American Physical Society ("APS") and Kayla Cerminara ("You") consists of your license details and the terms and conditions provided by the American Physical Society and SciPris.

Licensed Content Information

License Number:	RNP/22/APR/052535
License date:	12-Apr-2022
DOI:	10.1103/PhysRevB.51.6868
Title:	Quasiparticle band structure of bulk hexagonal boron nitride and related systems
Author:	X. Blase et al.
Publication:	Physical Review B
Publisher:	American Physical Society
Cost:	USD \$ 0.00

Request Details

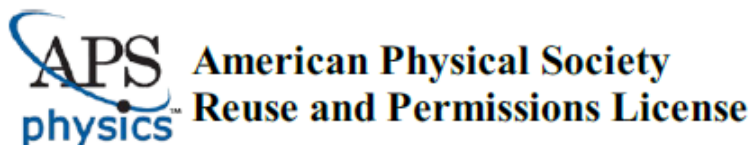
Does your reuse require significant modifications:	No
Specify intended distribution locations:	United States
Reuse Category:	Reuse in a thesis/dissertation
Requestor Type:	Student
Items for Reuse:	Figures/Tables
Number of Figure/Tables:	1
Figure/Tables Details:	Figure 2a and 2b
Format for Reuse:	Print and Electronic
Total number of print copies:	Up to 1000

Information about New Publication:

University/Publisher:	University of Nevada, Las Vegas
Title of dissertation/thesis:	Towards highly sensitive capacitance measurements of a quantum anomalous Hall phase in van der Waals heterostructures
Author(s):	Kayla Cerminara
Expected completion date:	May, 2022

License Requestor Information

Name:	Kayla Cerminara
Affiliation:	Individual
Email Id:	kcermina@unlv.nevada.edu
Country:	United States



TERMS AND CONDITIONS

The American Physical Society (APS) is pleased to grant the Requestor of this license a non-exclusive, non-transferable permission, limited to Print and Electronic format, provided all criteria outlined below are followed.

1. You must also obtain permission from at least one of the lead authors for each separate work, if you haven't done so already. The author's name and affiliation can be found on the first page of the published Article.
2. For electronic format permissions, Requestor agrees to provide a hyperlink from the reprinted APS material using the source material's DOI on the web page where the work appears. The hyperlink should use the standard DOI resolution URL, <http://dx.doi.org/{DOI}>. The hyperlink may be embedded in the copyright credit line.
3. For print format permissions, Requestor agrees to print the required copyright credit line on the first page where the material appears: "Reprinted (abstract/excerpt/figure) with permission from [(FULL REFERENCE CITATION) as follows: Author's Names, APS Journal Title, Volume Number, Page Number and Year of Publication.] Copyright (YEAR) by the American Physical Society."
4. Permission granted in this license is for a one-time use and does not include permission for any future editions, updates, databases, formats or other matters. Permission must be sought for any additional use.
5. Use of the material does not and must not imply any endorsement by APS.
6. APS does not imply, purport or intend to grant permission to reuse materials to which it does not hold copyright. It is the requestor's sole responsibility to ensure the licensed material is original to APS and does not contain the copyright of another entity, and that the copyright notice of the figure, photograph, cover or table does not indicate it was reprinted by APS with permission from another source.
7. The permission granted herein is personal to the Requestor for the use specified and is not transferable or assignable without express written permission of APS. This license may not be amended except in writing by APS.
8. You may not alter, edit or modify the material in any manner.
9. You may translate the materials only when translation rights have been granted.
10. APS is not responsible for any errors or omissions due to translation.
11. You may not use the material for promotional, sales, advertising or marketing purposes.
12. The foregoing license shall not take effect unless and until APS or its agent, Aptara, receives payment in full in accordance with Aptara Billing and Payment Terms and Conditions, which are incorporated herein by reference.
13. Should the terms of this license be violated at any time, APS or Aptara may revoke the license with no refund to you and seek relief to the fullest extent of the laws of the USA. Official written notice will be made using the contact information provided with the permission request. Failure to receive such notice will not nullify revocation of the permission.
14. APS reserves all rights not specifically granted herein.
15. This document, including the Aptara Billing and Payment Terms and Conditions, shall be the entire agreement between the parties relating to the subject matter hereof.

Bibliography

- [1] Vila, M., Garcia, J. H. & Roche, S. Valley-polarized quantum anomalous hall phase in bilayer graphene with layer-dependent proximity effects. *Physical Review B* **104** (2021).
- [2] Castro Neto, A. H., Guinea, F., Peres, N. M. R., Novoselov, K. S. & Geim, A. K. The electronic properties of graphene. *Reviews of Modern Physics* **81**, 109–162 (2009).
- [3] Liu, G.-B., Shan, W.-Y., Yao, Y., Yao, W. & Xiao, D. Three-band tight-binding model for monolayers of group-VIB transition metal dichalcogenides. *Physical Review B* **88**, 085433 (2013).
- [4] Bhimanapati, G., Glavin, N. & Robinson, J. 2D Boron Nitride. In *Semiconductors and Semimetals*, vol. 95, 101–147 (Elsevier, 2016).
- [5] Blase, X., Rubio, A., Louie, S. G. & Cohen, M. L. Quasiparticle band structure of bulk hexagonal boron nitride and related systems. *Physical Review B* **51**, 6868–6875 (1995).
- [6] Hasan, M. Z. & Kane, C. L. *Colloquium* : Topological insulators. *Reviews of Modern Physics* **82**, 3045–3067 (2010).
- [7] Qi, X.-L. & Zhang, S.-C. Topological insulators and superconductors. *Reviews of Modern Physics* **83**, 1057–1110 (2011).
- [8] Ren, Y., Qiao, Z. & Niu, Q. Topological phases in two-dimensional materials: a review. *Reports on Progress in Physics* **79**, 066501 (2016).
- [9] Liu, C.-X., Zhang, S.-C. & Qi, X.-L. The Quantum Anomalous Hall Effect: Theory and Experiment. *Annual Review of Condensed Matter Physics* **7**, 301–321 (2016).
- [10] Klitzing, K. v., Dorda, G. & Pepper, M. New Method for High-Accuracy Determination of the Fine-Structure Constant Based on Quantized Hall Resistance. *Physical Review Letters* **45**, 494–497 (1980).
- [11] Yu, R. *et al.* Quantized Anomalous Hall Effect in Magnetic Topological Insulators. *Science* **329**, 61–64 (2010).
- [12] Haldane, F. D. M. Model for a Quantum Hall Effect without Landau Levels: Condensed-Matter Realization of the "Parity Anomaly". *Physical Review Letters* **61**, 2015–2018 (1988).

- [13] Onoda, M. & Nagaosa, N. Quantized Anomalous Hall Effect in Two-Dimensional Ferromagnets: Quantum Hall Effect in Metals. *Physical Review Letters* **90**, 206601 (2003).
- [14] Qi, X.-L., Hughes, T. L. & Zhang, S.-C. Topological field theory of time-reversal invariant insulators. *Physical Review B* **78**, 195424 (2008).
- [15] Chang, C.-Z. *et al.* Experimental Observation of the Quantum Anomalous Hall Effect in a Magnetic Topological Insulator. *Science* **340**, 167–170 (2013).
- [16] Novoselov, K. S. *et al.* Electric Field Effect in Atomically Thin Carbon Films. *Science* **306**, 666–669 (2004).
- [17] Sichau, J. *et al.* Resonance Microwave Measurements of an Intrinsic Spin-Orbit Coupling Gap in Graphene: A Possible Indication of a Topological State. *Physical Review Letters* **122**, 046403 (2019).
- [18] Geim, A. K. & Grigorieva, I. V. Van der Waals heterostructures. *Nature* **499**, 419–425 (2013).
- [19] Huang, B. *et al.* Emergent phenomena and proximity effects in two-dimensional magnets and heterostructures. *Nature Materials* **19**, 1276–1289 (2020).
- [20] Island, J. O. *et al.* Spin-orbit-driven band inversion in bilayer graphene by the van der Waals proximity effect. *Nature* **571**, 85–89 (2019).
- [21] Luryi, S. Quantum capacitance devices. *Applied Physics Letters* **52**, 501–503 (1988).
- [22] Eisenstein, J. P., Pfeiffer, L. N. & West, K. W. Negative compressibility of interacting two-dimensional electron and quasiparticle gases. *Physical Review Letters* **68**, 674–677 (1992).
- [23] Yu, G. *et al.* Interaction phenomena in graphene seen through quantum capacitance. *Proceedings of the National Academy of Sciences* **110**, 3282–3286 (2013).
- [24] Hall, E. H. *et al.* On a new action of the magnet on electric currents. *American Journal of Mathematics* **2**, 287–292 (1879).
- [25] Karsenty, A. A comprehensive review of integrated hall effects in macro-, micro-, nanoscales, and quantum devices. *Sensors* **20**, 4163 (2020).
- [26] Sinitsyn, N. A. Semiclassical theories of the anomalous Hall effect. *Journal of Physics: Condensed Matter* **20**, 023201 (2008). ArXiv: 0712.0183.
- [27] Nagaosa, N., Sinova, J., Onoda, S., MacDonald, A. H. & Ong, N. P. Anomalous hall effect. *Reviews of modern physics* **82**, 1539 (2010).
- [28] Datta, S. 7.3.1 Quantum Capacitance. In *Lessons From Nanoelectronics: A New Perspective On Transport (Second Edition) - Part A: Basic Concepts*, 85–88 (World Scientific Publishing Company, 2012), second edn.

- [29] An, Z., Liu, F. Q., Lin, Y. & Liu, C. The universal definition of spin current. *Scientific Reports* **2**, 388 (2012).
- [30] Wallace, P. R. The band theory of graphite. *Physical Review* **71**, 622–634 (1947).
- [31] Wang, Q. H., Kalantar-Zadeh, K., Kis, A., Coleman, J. N. & Strano, M. S. Electronics and optoelectronics of two-dimensional transition metal dichalcogenides. *Nature Nanotechnology* **7**, 699–712 (2012).
- [32] Zhu, Z. Y., Cheng, Y. C. & Schwingenschlögl, U. Giant spin-orbit-induced spin splitting in two-dimensional transition-metal dichalcogenide semiconductors. *Physical Review B* **84**, 153402 (2011).
- [33] Mag-isa, A. E., Kim, J.-H., Lee, H.-J. & Oh, C.-S. A systematic exfoliation technique for isolating large and pristine samples of 2d materials. *2D Materials* **2**, 034017 (2015).
- [34] Li, H. *et al.* Rapid and reliable thickness identification of two-dimensional nanosheets using optical microscopy. *ACS Nano* **7**, 10344–10353 (2013).
- [35] Bing, D. *et al.* Optical contrast for identifying the thickness of two-dimensional materials. *Optics Communications* **406**, 128–138 (2018).
- [36] Ni, Z. H. *et al.* Graphene thickness determination using reflection and contrast spectroscopy. *Nano Letters* **7**, 2758–2763 (2007).
- [37] Wang, L. *et al.* One-dimensional electrical contact to a two-dimensional material. *Science* **342**, 614–617 (2013).
- [38] Frisenda, R. *et al.* Recent progress in the assembly of nanodevices and van der waals heterostructures by deterministic placement of 2d materials. *Chemical Society Reviews* **47**, 53–68 (2018).
- [39] Haley, K. L. *et al.* Heated Assembly and Transfer of Van der Waals Heterostructures with Common Nail Polish. *Nanomanufacturing* **1**, 49–56 (2021).
- [40] Sulpizio, J. A., Hazeghi, A., Diankov, G., Goldhaber-Gordon, D. & Wong, H.-S. P. An integrated capacitance bridge for high-resolution, wide temperature range quantum capacitance measurements. *Review of Scientific Instruments* **82**, 053904 (2011). ArXiv: 1009.5407.
- [41] Verbiest, G. J. *et al.* Integrated impedance bridge for absolute capacitance measurements at cryogenic temperatures and finite magnetic fields. *Review of Scientific Instruments* **90**, 084706 (2019).
- [42] Young, A. F. & Levitov, L. S. Capacitance of graphene bilayer as a probe of layer-specific properties. *Physical Review B* **84**, 085441 (2011).
- [43] Ashoori, R. C. *et al.* Single-electron capacitance spectroscopy of discrete quantum levels. *Physical Review Letters* **68**, 3088–3091 (1992).

- [44] Wang, Z. *et al.* Origin and magnitude of ‘designer’ spin-orbit interaction in graphene on semiconducting transition metal dichalcogenides. *Physical Review X* **6**, 041020 (2016).
- [45] Wakamura, T. *et al.* Spin-orbit interaction induced in graphene by transition metal dichalcogenides. *Physical Review B* **99**, 245402 (2019).
- [46] David, A., Rakyta, P., Kormányos, A. & Burkard, G. Induced spin-orbit coupling in twisted graphene–transition metal dichalcogenide heterobilayers: Twistronics meets spintronics. *Physical Review B* **100**, 085412 (2019).
- [47] Li, Y. & Koshino, M. Twist-angle dependence of the proximity spin-orbit coupling in graphene on transition-metal dichalcogenides. *Physical Review B* **99**, 075438 (2019).
- [48] McGuire, M. A., Dixit, H., Cooper, V. R. & Sales, B. C. Coupling of crystal structure and magnetism in the layered, ferromagnetic insulator CrI_3 . *Chemistry of Materials* **27**, 612–620 (2015).
- [49] Dillon Jr, J. & Olson, C. Magnetization, resonance, and optical properties of the ferromagnet CrI_3 . *Journal of Applied Physics* **36**, 1259–1260 (1965).
- [50] Shcherbakov, D. *et al.* Raman spectroscopy, photocatalytic degradation, and stabilization of atomically thin chromium tri-iodide. *Nano letters* **18**, 4214–4219 (2018).
- [51] Wang, X., Sun, Y. & Liu, K. Chemical and structural stability of 2d layered materials. *2D Materials* **6**, 042001 (2019).

Curriculum Vitae

Kayla Cerminara
kayla.cerminara@gmail.com

EDUCATION

GRADUATE:

M.Sc. in Physics at University of Nevada, Las Vegas (UNLV) *Current*
Thesis topic: Towards highly sensitive capacitance measurements of a quantum anomalous Hall phase in van der Waals heterostructures.

UNDERGRADUATE:

B.Sc. in Physics at University of Nevada, Las Vegas *May 2020*
Minor: Mathematics
Research: Towards passivation techniques for two-dimensional ferromagnetic chromium tri-iodide.

RESEARCH INTERESTS

My research interests span over the field of condensed matter physics. Specifically, I study materials on the nanoscale. I started my interest for 2-dimensional materials in my undergraduate career where I studied the degradation of materials and the effect on their electronic properties. Currently, I am looking at synthetic topological phases in van der Waals heterostructures.

EXPERIENCE

Graduate Research Assistant (UNLV) under Dr. Joshua Island *August 2020 - present*
- Research for graduate degree.
Graduate Assistant (UNLV) *August 2020 - present*
- Instruction of intro-level physics labs.

Annual Graduate & Professional Research Forum
Research Forum

April 3, 2021

- Conference poster: *“Towards highly sensitive capacitance measurements of 2D materials”*

Undergraduate Research Assistant (UNLV) under Dr. Joshua Island *August 2019 - May 2020*

- Research for undergraduate degree

Teaching Assistant

August 2018 - December 2019

- Graded astronomy exams (AST 103).

ACHIEVEMENTS

Graduate Assistantship (UNLV)

Fall 2020 - Spring 2022

Society of Physics Students member (UNLV)

2017-2020

Dean's Honor List (UNLV)

Spring 2020, Fall 2019

Dean's List (College of Southern Nevada)

Spring 2016, Spring 2015, Fall 2016

PERSONAL NOTE

Outside of academia, I enjoy fitness and getting outdoors. I am constantly looking for a good hike or adventure with my husband and dog.

PUBLICATIONS

(1) Haley, K.L.; Cloninger, J.A.; Cerminara, K.; Sterbentz, R.M.; Taniguchi, T.; Watanabe, K.; Island, J.O. Heated Assembly and Transfer of Van der Waals Heterostructures with Common Nail Polish.
<https://doi.org/10.3390/nanomanufacturing1010005> *Nanomanufacturing* **1**, 49-56 (2021).